Tectonic evolution of the Indio Hills segment of the San Andreas fault in southern California, southwestern USA

Jean-Baptiste P. Koehl[1,2,3,4], Steffen G. Bergh[2,3], Arthur G. Sylvester[5]

1) Centre for Earth Evolution and Dynamics, (CEED), University of Oslo, N-0315 Oslo, Norway.

2) Department of Geosciences, UiT The Arctic University of Norway in Tromsø, N-9037 Tromsø, Norway.

3) Research Center for Arctic Petroleum Exploration (ARCEx), UiT The Arctic University of Norway.

4) CAGE – Centre for Arctic Gas Hydrate, Environment and Climate, UiT The Arctic University of Norway.

5) Department of Earth Science, University of California, Santa Barbara, USA.

Correspondence: jeanbaptiste.koehl@gmail.com

Abstract

Transpressional uplift domains of invertedPliocene–Pleistocene basin fill along the San Andreas fault zone in Coachella Valley, southern California (USA), are characterized by fault linkage and segmentation and deformation partitioning. The Indio Hills wedge-shaped uplift block is located in between two boundary fault strands, the Indio Hills fault to the northeast and the main San Andreas fault to the southwest, which merge to the southeast. Uplift commenced about or later than 0.76 million years ago and involved progressive fold and faulting stages caused by a change from distributed strain to partly partitioned right-slip and reverse/thrust displacement on the bounding faults when approaching the fault junction. Major fold structures in the study area include oblique, right-stepping, partly overturned *en echelon* macro-folds that tighten and bend into parallelism with the Indio Hills fault to the east and become more open towards the main San Andreas fault to the west, indicating an early and close relationship of the macro-folds with the Indio Hills fault and a late initiation of the main San Andreas fault. Sets of strike-slip to reverse step-over and right- and left-lateral cross faults and conjugate kink bands affect the entire uplifted area, and locally offset the *en echelon* macro-folds. Comparison with the Mecca Hills and Durmid Hills uplifts farther southeast along strike in Coachella Valley reveals notable similarities, but also differences in fault architectures, spatial and temporal evolution, and deformation mechanisms. The present work contributes to better understand the structure and tectonic history of a major fault system along a transform plate boundary.

Introduction

This paper describes and evaluates structural patterns of the Indio Hills uplift in the northwestern part of Coachella Valley along the San Andreas fault zone (SAFZ) in California, southwestern USA (Fig. 1), where the fold–fault architecture, evolution, and partitioning of deformation compared to Mecca Hills and Durmid Hills are not well understood (e.g., Keller et al., 1982, Dibblee and Minch, 2008). The main goal of this study is to analyze internal macro- and meso-scale folds and related faults and to outline the kinematic evolution in relation to major SAFZ-related fault strands in the area (Fig. 1: Keller et al., 1982; Guest et al., 2007). These include the Indio Hills fault in the northeast (Allen, 1957; Tyley, 1974), and the main San Andreas fault along the southwest flank of the Indio Hills and of the Mecca Hills, and along the northeast flank of the Durmid Hills (Janecke et al., 2018; Fig. 1). The progressive tectonic evolution model for the Indio Hills uplift is then compared and correlated with other major uplifts and SAFZ-related fault strands along strike in the Mecca Hills and Durmid Hills (Sylvester and Smith, 1987; McNabb et al., 2017; Janecke et al., 2018; Bergh et al., 2019). We also discuss briefly the potential northwestward continuation of the Indio Hills fault into the Eastern California shear zone and its role as possible transfer fault (Dokka and Travis, 1990a, 1990b; Thatcher et al., 2016). The variable fault and fold architectures and associated ongoing seismic activity in these uplift areas underline the need for persistent along-strike studies of the SAFZ to characterize the fundamental geometry, resolve the kinematic development, and correlate regionally major fault strands (cf. Janecke et al., 2018). Such studies are essential to explain the observed lateral variations in fold and fault architectures and to resolve mechanisms of transpression, fault linkage, and areal segmentation in continental transform settings.

Geological setting

The Coachella Valley segment of the SAFZ in southern California is expressed as multiple, right-lateral fault strands, which uplifted blocks in the Indio Hills, Mecca Hills, and Durmid Hills (Fig. 1; Sylvester, 1988). These domains comprise thick successions of Pliocene–Pleistocene sedimentary strata uplifted and deformed in Pleistocene–Holocene time due to oblique convergence of the Pacific and North American plates and movement along the SAFZ and related faults (e.g., Atwater and Stock, 1998; Spotila et al., 2007; Dorsey et al., 2011). Recent structural studies in the Mecca Hills (McNabb et al., 2017; Bergh et al., 2019), and Durmid Hills at the southern termination of the SAFZ (Janecke et al., 2018), show that

66 individual fault strands are linked, and that the deformation splits into abruptly changing fold

67 and fault geometries (Fuis et al., 2012, 2017). These recent works call for further

68 characterization of the understudied Indio Hills segment in order to compare its structural

69 development with other uplifted features along a major transform plate boundary fault zone.

70 Below we summarize local and regional fault nomenclature, distribution, and fault movement

71 history (Table 1) throughout the greater Coachella Valley region (Fig. 1), the stratigraphy of

72 the Indio Hills area, and previous structural work in the main Indio Hills, Mecca Hills, and

73 Durmid Hills uplift areas.

74

75 *Regional faults*

76 The southeastern Indio Hills are a WNW–ESE–trending tectonic uplift situated in a

77 small restraining bend northeast of the main San Andreas fault (Figs. 1 and 2 and Supplement

78 S1). The studied uplift is located along strike about 25–50 kilometers northwest of the Mecca

79 Hills and Durmid Hills, and to the southeast of the major left bend in the SAFZ trace near San

80 Gorgonio Pass (Matti et al., 1985, 1992; Matti and Morton, 1993; Dair and Cooke, 2009).

81 The main faults in the southeastern Indio Hills include the Indio Hills fault in the

82 northeast (Allen, 1957; Tyley, 1974), and the main San Andreas fault in the southwest (we

83 refrain from using the name "Indio strand" ascribed to this fault by Gold et al., 2015 to avoid

84 confusion with the Indio Hills fault). Regionally, the Indio Hills fault possibly merges with

85 the Landers–Mojave Line and the Eastern California shear zone in the north (Dokka and

86 Travis, 1990a, 1990b; Nur et al., 1993a, 1993b; Thatcher et al., 2016). The Landers–Mojave

87 Line is believed to be the locus of several recent earthquakes aligned in a NNW–SSE-trend,

88 including the 1992 Joshua Tree earthquake (Fig. 1b; Nur et al., 1993a, 1993b). These

89 earthquakes were tentatively ascribed to movement along a through-going NNW–SSE-

90 striking fault, possibly the west-dipping, Quaternary West Deception Canyon fault (Sieh et

91 al., 1993; Rymer, 2000). This fault is thought to crosscut the E–W- to ENE–WSW-striking,

92 left-lateral, Holocene Pinto Mountain fault, which merges with the main strand of the San

93 Andreas fault in the west at the intersection of the right-lateral Mission Creek and Mill Creek

94 strands (Allen, 1957; Bryant, 2000; Kendrick et al., 2015; Blisniuk et al., 2021). The former is

95 thought to correspond to the continuation of the main San Andreas fault to the northwest

96 (Gold et al., 2015) and may have accommodated ca. 89 km of right slip in the past 4 million

97 years, whereas the latter accommodated about 8 km right slip at 0.5–0.1 Ma and is offset ca. 1

98 km by the Pinto Mountain fault (Kendrick et al., 2015).

99   The main San Andreas fault continues to the southeast where it bounds the Mecca

100   Hills to the southwest. The Painted Canyon fault, a previous (late Miocene?–) Pliocene

101   southwest-dipping normal fault reactivated as a right-lateral-reverse oblique-slip fault in the

102   Pleistocene–present-day, bounds the Mecca basin to the northeast (Sylvester and Smith, 1987;

103   McNabb et al., 2017; Bergh et al., 2019). Farther southeast, the main San Andreas fault

104   proceeds along the northeast flank of the Durmid Hills opposite the Pleistocene (ca. 1 Ma),

105   right-lateral East Shoreline fault (Babcock, 1969, 1974; Bürgmann, 1991; Janecke et al.,

106   2018). There, the main San Andreas fault merges with the Brawley seismic zone (Lin et al.,

107   2007; Hauksson et al., 2012; Lin, 2013) and, together with the right-lateral San Jacinto fault

108   zone, they merge into the right-lateral Imperial fault (Rockwell et al., 2011). In the north, the

109   main San Andreas fault splays into the Banning strand and the Mission Creek fault in the

110   northwestern part of the Indio Hills (Keller et al., 1982; Gold et al., 2015). The Banning

111   strand is much younger than the Mission Creek fault and may have accommodated

112   approximately 3 km of right slip in the past 0.1 million years (Kendrick et al., 2015).

113   Northwest and west of the Coachella Valley, Miocene–Pleistocene sedimentary strata

114   are structurally bounded by the San Bernardino and San Jacinto fault strands of the SAFZ

115   (Bilham and Williams, 1985; Matti et al., 1985; Morton and Matti, 1993; Spotila et al., 2007).

116   To the southwest, Miocene–Pleistocene strata are bounded by the West Salton Detachment

117   fault (Dorsey et al., 2011). The San Jacinto fault is typically believed to have slipped ca. 25

118   km right-laterally in the past 1.5 million years (Matti and Morton, 1993; Kendrick et al.,

119   2015), whereas the West Salton Detachment fault is a low-angle normal fault that

120   accumulated ca. 8–10 km of normal-oblique movement starting in the mid Miocene and is

121   related to the opening of the Gulf of California (Prante et al., 2014 and references therein).

122

Stratigraphy of the Indio Hills and adjacent areas

124   The Indio Hills uplift is an inverted Pliocene–Pleistocene sedimentary basin lying

125   upon Mesozoic granitic basement rocks, which we regard as an analog to the inverted Mecca

126   basin farther southeast (Keller et al., 1982; Damte, 1997; McNabb et al., 2017; Bergh et al.,

127   2019). In the Mecca basin, alluvial, fluvial and lacustrine deposits of the Mecca and Palm

128   Spring formations are truncated unconformably by the mid to upper Pleistocene Ocotillo

129   Formation (Dibblee, 1954; Sylvester and Smith, 1976, 1987; Boley et al., 1994; Rymer, 1994;

130   Sheridan et al., 1994; Sheridan and Weldon, 1994; Winker and Kidwell, 1996; Kirby et al.,

131   2007; McNabb et al., 2017; Table 1). Similar uplifted strata at Durmid Hills (Fig. 1) belong to

132   the Pliocene–Pleistocene Borrego Formation, and are overlain by mid to upper Pleistocene

133   deposits of the Brawley and Ocotillo formations (Dibblee, 1997; Herzig et al., 1988; Lutz et

134   al., 2006; Kirby et al., 2007; Dibblee and Minch, 2008).

135   Leuco-granitic rocks crop out near gently SW-dipping conglomerates along the

136   northeastern flank of the Indio Hills, near the trace of the Indio Hills fault (Fig. 2). Despite

137   proximity of the conglomerates with segmented granite outcrops, the contact itself is not

138   exposed. The conglomerates are the lowermost stratigraphic unit exposed in the Indio Hills

139   and are characterized by a succession of meter-thick beds of very coarse, poorly sorted blocks

140   of gneissic and granitic rocks more than a meter in size. Previous mapping in the area

141   (Dibblee, 1954; Lancaster et al., 2012) considered the conglomerates as stratigraphic

142   equivalents to the mid to upper Pliocene Mecca Formation in the Mecca Hills (Sylvester and

143   Smith, 1987; McNabb et al., 2017; Bergh et al., 2019) and that at least part of the clasts are

144   from the leuco-granitic rocks, which must correspond to basement rocks of the inverted Indio

145   Hills basin. Up-section toward the southwest the conglomerate gradually is succeeded by

146   coarse-grained sandstone, which defines the transition from the Mecca Formation to the lower

147   Palm Spring Formation.

148   The Palm Spring Formation in the Indio Hills consists of moderately- to well-

149   consolidated alluvial fan deposits (Dibblee and Minch, 2008), with some interbedded gypsum

150   layers and red-colored calcareous mudstone, as in the Mecca Hills (Sylvester and Smith,

151   1987). The main rock types include beds of light-colored, medium- to coarse-grained

152   sandstone, gray–brown silty sandstone, and dark biotite-rich mudstone. The southwestwards

153   increase in silt–clay toward the main San Andreas fault (also recorded in the Mecca Hills;

154   Bergh et al., 2019) may indicate a gradual transition from the lower to the upper member of

155   the Palm Spring Formation. By contrast, the transition between the lower and upper members

156   of the Palm Spring Formation in the Mecca Hills is marked by two angular unconformities

157   that signal further steps in uplift and inversion of the Mecca basin (Table 1; McNabb et al.,

158   2017; Bergh et al., 2019).

159   Ages of 3.0-2.3 Ma (latest Pliocene–early Pleistocene) and 2.6–0.76 Ma (earliest

160   Pleistocene to earliest late Pleistocene), were obtained respectively for the lower and upper

161   member of the Palm Spring Formation in the Mecca Hills based on reversed magnetic polarity

162   data (Chang et al., 1987; Boley et al., 1994; McNabb, 2013; McNabb et al., 2017; Table 1).

163   We infer a similar age range for the Palm Spring Formation in the southern Indio Hills.

164   In contrast to other uplift areas in Coachella Valley, the Ocotillo Formation has not

165   been mapped in the Indio Hills in the present study. However, based on the occurrence of the

166   Bishop Ash at the northwestern edge of the study area and on the occurrence of the volcanic

deposit within the uppermost Palm Spring Formation or at the base of the overlying Ocotillo

Formation in the Mecca Hills, it is likely that the Ocotillo Formation is present just northwest

of the area mapped (Fig. 2). In addition, it is deposited on the flank northeast of the Indio

Hills fault, and southwest of the main San Andreas fault (Figs. 1 and 2), indicating that this

unit was either not deposited or eroded in the area that recorded the most uplift in Indio Hills.

Additional dating constraints on transpressional uplift in the Coachella Valley include

tephrochonology of the 0.765 million year old Bishop Ash layer (Sarna-Wojcicki et al., 2000;

Zeeden et al., 2014; Table 1). This volcanic deposit is found within the upper member of the

Palm Spring Formation (which is unconformably overlain by the Ocotillo Formation) in the

hanging wall of the Painted Canyon fault away from the fault, and within the base of the

Ocotillo Formation in the hanging wall of the Painted Canyon fault near the fault (Ocotillo

and uppermost Palm Spring formations interfingering near the fault) and in the footwall of the

fault (McNabb et al., 2017; Bergh et al. 2019). The unconformable contact between the Palm

Spring and Ocotillo formations away from the Painted Canyon fault towards the southwest

and their interfingering relationship near the fault suggest that uplift had already initiated prior

to deposition of the Ocotillo Formation (i.e., before 0.76 Ma, in the mid Pleistocene), possibly

during the formation of the lower unconformity between the lower and upper members of the

Palm Spring Formation (McNabb et al., 2017; Table 1). Complementarily, the involvement of

the Bishop Ash in deformation suggest that deformation continued past 0.76 Ma (in the late

Pleistocene).

Major tectonic uplifts in the Coachella Valley

Indio Hills

The southeastern end of the Indio Hills is an uplifted domain of deformed strata of the

Mecca and Palm Spring formations situated in between the main San Andreas and Indio Hills

fault (Fig. 2). The main San Andreasfault corresponds to a major oblique strike-slip fault

segment at the eastern end of San Gorgonio Pass (Matti et al., 1985; Morton et al, 1987). It is

easily traced to Indio Hills (Figs. 1 and 2) since its main trace provides preferential pathways

for ground water flow and growth of wild palm trees along strike.

The Indio Hills fault was mapped north of the study area (Dibblee and Minch, 2008)

extending into the Landers–Mojave Line (Nur et al., 1993a, 1993b), a NNW–SSE-striking

right-lateral fault system extending hundreds of kilometers northward from the southeastern

Indio Hills into the Eastern California shear zone and related fault segments such as the

Calico and Camp Rock faults (Fig. 1; Dokka et al., 1990a; Nur et al. 1993b). The Indio Hills

201 fault may correspond to a major fault splay of the SAFZ (Dokka and Travis, 1990a, 1990b;

202 Thatcher et al., 2016). Southeast of the Indio Hills, however, the geometry of the Indio Hills

203 fault remains elusive, and the fault either dies out or merges with structures like the main San

204 Andreas fault, the Skeleton Canyon fault, and/or the Painted Canyon fault in the Mecca Hills

205 (Fig.1).

206   The transpressional character of the Indio Hills uplift was suggested by Sylvester and

207 Smith (1987). However, detailed structural analyses documenting this hypothesis for the uplift

208 as a whole have not been conducted. Gold et al. (2015) explore tectonogeomorphic evidence

209 for dextral-oblique uplift and Keller et al. (1982) and Blisniuk et al. (2021) focus on landscape

210 evolution near the intersection of the Banning strand and Mission Creek fault (northwest of

211 the study area), which merge into the main San Andreas fault (Fig. 1). In addition to

212 investigating soil profiles, offset drainage systems, and recent (a few thousand years old)

213 displacement along the SAFZ, Keller et al. (1982) called attention to a strong dominance of

214 gently plunging and upright macro-folds in bedrock strata along the Mission Creek fault and

215 at the southeastern end of the Banning strand where these faults merge. Their study showed

216 that bends and steps along the main fault traces were consistently located near brittle fault

217 segments and zones of uplift. The study also showed that drainage systems were offset

218 recently (at ca. 0.03–0.02 Ma) and indicate relatively high slip rates along the Mission Creek

219 fault in the order of 23–35 cm.y^{-1}, i.e., comparable to the more recent c. 23 cm.y^{-1} estimate by

220 Blisniuk et al. (2021).

221 *Mecca Hills*

222   Farther south, the Mecca Hills uplift was previously defined as a classic flower-

223 structure (Sylvester and Smith, 1976, 1987; Sylvester, 1988), in which all folds and faults

224 formed synchronously and merged at depth. Recent analyses (Bergh et al., 2014, 2019)

225 indicate that a modified flower-like structure, consisting of a steep SAFZ fault core zone to

226 the southwest, a surrounding approximately one–two kilometers wide damage zone expressed

227 by *en echelon* folds and faults oblique to the SAFZ (including left-slip cross faults), steeply

228 plunging folds, and SAFZ-parallel fold and thrust belt features (including right- and left-slip

229 and oblique-reverse faults) formed in kinematic succession. In addition to the steep shallow

230 portion of the SAFZ (Fuis et al., 2012, 2017), two other, major NW–SE-striking faults occur

231 in the Mecca Hills (Fig. 1). One is the Skeleton Canyon fault, which initiated as a steep

232 SAFZ-parallel strike-slip fault and was reactivated as a reverse fault dipping gently

233 northeastwards in the late kinematic stages (Sylvester and Smith, 1976, 1979, 1987; Bergh et

234 al., 2019). The other is the Painted Canyon fault, which is a former Miocene–Pliocene basin-

235   bounding normal fault (McNabb et al., 2017) and is now reactivated as a NE-directed thrust

236   fault with dip to the southwest (Bergh et al., 2019; Table 1). The polyphase evolution and

237   reactivation of internal oblique, step-over faults, and SAFZ-parallel faults, were explained by

238   a series of successive–overlapping events involving a change from distributed, locally

239   partitioned, into fully partitioned strain in a changing, oblique-plate convergence regime

240   (Bergh et al., 2019).

241   *Durmid Hills*

242   The Durmid Hills are an elongate ridge that parallels the main strand of the SAFZ at

243   the south edge of the Salton Sea in Imperial Valley (Fig. 1). Farther south, this deformation

244   zone and the SAFZ project towards the Brawley seismic zone, an oblique, transtensional rift

245   area with particularly high seismicity (Lin et al., 2007; Hauksson et al., 2012; Lin, 2013). The

246   main San Andreas fault (mSAF) is located on the northeast side of the Durmid Hills and has

247   been thoroughly studied (Dibblee, 1954, 1997; Babcock, 1969, 1974; Bilham and Williams,

248   1985; Bürgmann, 1991; Sylvester et al., 1993; Lindsey and Fialko, 2013; Janecke et al.,

249   2018). The rocks southwest of the mSAF consist of highly folded Pliocene–Pleistocene

250   deposits (Babcock, 1974; Bürgmann, 1991; Markowski, 2016; Janecke et al., 2018) bounded

251   to the southwest by the subsidiary East Shoreline fault strand of the SAFZ. Northeast of the

252   mSAF, the formations are much less deformed (Janecke et al., 2018). The overall structure

253   (Fig. 1) resembles a right-lateral strike-slip duplex (Sylvester, 1988), but the geometry is not

254   fully consistent with a duplex model due to abundant left-lateral cross faults and internal

255   block rotations. Instead, the Durmid Hills structure was interpreted as a ladder structure

256   (Janecke et al., 2018), as defined by Davis (1999) and Schulz and Balasko (2003), where

257   overlapping, E–W- to NW–SE-striking step-over faults rotated along multiple connecting

258   cross faults. The one–three kilometers wide Durmid ladder structure consists of multiple

259   internal, clockwise-rotating blocks bounded by major *en echelon* folds and right- and left-

260   lateral cross faults in between the right-slip mSAF and East Shoreline fault strand, indicating

261   a complex termination of the SAFZ around the Brawley Seismic Zone to the southeast

262   (Fig.1).

263

264   **Methods and data**

265   In our investigation of the Indio Hills, we used Google Earth images and aerial

266   photographs (© Google Earth 2011) as a basis for detailed field and structural analyses (Fig.

267   2). We mapped and analyzed individual macro- and meso-scale folds and associated faults in

268   Miocene–Pliocene strata both in the field and via imagery analysis. Key horizons of light-

269   colored quartz sandstone and carbonate rocks in the Palm Spring Formation provide structural

270   markers, notably to correlate bed displacement and fault–fold geometries and kinematics. We

271   address crosscutting relations of the main San Andreas and Indio Hills faults and nearby fold

272   structures. Structural orientation data are obtained from meso-scale folds and faults and are

273   integrated between the areal segments to link a prevalent pattern of deformation into a wider

274   structural architecture (Fig. 2).

275

276   **Results**

277   *Structural overview of the Indio Hills*

278   The study area comprises three major, SAFZ-oblique, asymmetric, E–W-trending,

279   moderately west-plunging fold systems having multiple smaller-scale parasitic folds (Fig. 2).

280   The main folds affect most of the Palm Spring Formation in a zone approximately two

281   kilometers wide between the main San Andreas and Indio Hills faults (Fig. 2). The

282   northeastern flank of the Indio Hills is structurally different by consisting of a sub-horizontal,

283   NW–SE-trending, open, upright anticline, which trends parallel to the Indio Hills fault (Fig.

284   2). Similarly, close to the main San Andreas fault, tilted strata of the Palm Spring Formation

285   are folded into a tight, steeply plunging shear fold (folds involving shearing along a plane that

286   is parallel to subparallel to the fold's axial plane; Groshong, 1975; Meere et al., 2013; Fig. 2).

287   At smaller scale, several subsidiary reverse faults and mostly right-slip, step-over faults

288   having orientations both parallel with (E–W to NW–SE) and perpendicular (NNE–SSW) to

289   the bounding faults exist within the macro-folded domain. Most of these faults truncate

290   individual SAFZ-oblique folds.

291

292   *SAFZ-oblique macro-folds*

293   SAFZ-oblique macro-folds are consistently asymmetric and mostly south-verging, and

294   their axial surfaces are arcuate and right-stepping (Fig. 2). Fold geometries change from open

295   and nearly upright near the main San Andreas fault, to kink/chevron styles in the middle part,

296   to very tight (isoclinal) and overturned fold styles adjacent to the Indio Hills fault (Fig. 3a–c

297   and Supplement S2a–c). These changes in geometry correspond to a change in obliquity of

298   the fold axial surface trace from approximately 60–70° to less than 20° with the Indio Hills

299   fault (Fig. 2). All three macro-folds have axial trends that bend and partly merge into

300   parallelism with the Indio Hills fault. In contrast, moderate to steeply WSW-dipping strata of

301   the Palm Spring Formation are obliquely truncated by the main San Andreas fault. Tighter

302   fold hinges are mapped in the central macro-fold and on the back-limb (stretched long limb in

an overturned fold) of the Z-shaped, southeastern macro-fold (Fig. 2). These folds were not observed northeast of the Indio Hills fault, nor southwest of the main San Andreas fault.

Northwestern and central macro-folds

The northwestern and central macro-folds define two major, compound and arcuate fold systems that affect the entire Palm Spring Formation between the main San Andreas and Indio Hills faults (Fig. 3a–b). They consist of eight subsidiary Z- and S-shaped, south-verging anticline-syncline pairs, and show fold axes plunging variably but mostly about 30° to the west (Fig. 2). At large scale, both folds tighten northeastward and display clockwise bend of axial traces from ENE–WSW near the main San Andreas fault, to E–W and NW–SE as they approach the Indio Hills fault (Fig. 2 and 3c). Fold hinges in the west are typically symmetric, concentric, and open (Supplement S3a–b), and become gradually tighter and dominantly Z-shaped kink folds eastward (Supplement S3c). The folds transform into tight, isoclinal, and inverted geometries (Supplement S3d–e) when approaching the central macro-fold back-limb (Fig. 3b), and they potentially merge with the SAFZ-parallel anticline less than 200 meters from the Indio Hills fault (Fig. 2). From southwest to northeast, the central macro-fold hinge zone displays a corresponding change in geometry, i.e., from symmetric, to kink/chevron, and to isoclinal overturned styles (Supplement S4a–b), until the folds of the central macro-fold flank the back-limb of the southeastern macro-fold (Supplement S4c–d). Bedding surfaces on the fore-limb (the shortened, inverted limb indicating the direction of tectonic transport in an overturned fold) of the central macro-fold dip steeply or are inverted, whereas strata on the back-limb mostly dip gently to the north or northwest, i.e., at a high angle to the bounding faults, and gradually change to northward dip when approaching the Indio Hills fault (Fig. 3c).

Another feature of the central macro-fold is that it is offset by a system of both layer-parallel and bed-truncating faults (Fig. 3b). Strata east of the fault system are affected by a large shear fold having thickened hinges and thinned limbs. The next fold to the north-northeast changes from open to tight, overturned, and locally isoclinal (Supplement S4a–c), and merges with the inverted, NE-dipping back-limb of the southeastern macro-fold (Fig. 3c). Notably, the consistent eastward tightening of fold hinges occurs within the lower stratigraphic parts of the Palm Spring Formation, whereas conglomerates of the underlying Mecca Formation are only weakly folded (see Southeastern macro-fold section). Furthermore, beds in tighter folds (especially in relatively weak clayish–silty dark mudstone layers) are commonly accompanied by disharmonic folds and internal structural disconformities. By contrast, more rigid, and thicker sandstone beds are more commonly fractured.

Southeastern macro-fold

The southeastern macro-fold is expressed as a kilometer-wide, Z-shaped, open to tight, south-verging syncline-anticline pair showing moderately west-plunging axes and steeply north-dipping axial surfaces (Fig. 3c). Most of the Palm Spring Formation strata on the back-limb trend parallel to the Indio Hills fault and dip about 50–70° to the north, whereas strata in the hinge and fore-limb dip about 40–70° to the west/southwest (Fig. 3c). Combined with a relatively narrow hinge zone, these attitudes define the southeastern macro-fold as a chevron type. The axial trend of the syncline-anticline pair is at a low angle (< 20°) to the Indio Hills fault but bends into a NE–SW trend westward with a much higher (oblique) angle to the main San Andreas fault, which cuts off the fore-limb strata (Fig. 2). The southeastern macro-fold is very tight in the north and east and has several smaller-scale, tight to isoclinal, strongly attenuated folds on the main back-limb that merge from the central macro-fold, thus indicating increasing strain intensity northeastward (see discussion). In contrast to the tightly folded beds of the Palm Spring Formation, bedding surfaces in conglomerates of the underlying Mecca Formation are only weakly folded northeastward and becomes part of the open SAFZ-parallel anticline close to the Indio Hills fault.

A macro-folded siltstone layer of the lower Palm Spring Formation more than 200 meters southwest of the Indio Hills fault (Fig. 4a) contains centimeter-scale, upright (sub-horizontal) and disharmonic folds having E–W trend and western plunge (Fig. 4b). These intra-layer folded strata are cut by low-angle reverse faults yielding a NE-directed sense-of-shear. The upright geometry and the sub-horizontal fold axes (about 5° plunge) of these intra-bed minor folds differ from the SAFZ-oblique folds but resemble those of the macro-scale, SAFZ-parallel NW–SE-trending anticline near the Indio Hills fault. These disharmonic folds are interpreted as intra-detachment folds (see discussion).

SAFZ-parallel macro-folds

About 100–200 meters southwest of the trace of the Indio Hills fault, the conglomerates of the Mecca Formation are folded into a major open anticline, whose axis is parallel to slightly oblique (< 20°) to the Indio Hills fault. This macro-fold is traceable northwestward to where the Indio Hills fault bends northward (Fig. 1). The southwestern limb of the fold marks the transition from the Mecca Formation conglomerate with the overlying Palm Spring Formation on the back-limb of the southeastern and central macro-folds (Fig. 2 and Supplement S4c). The conglomerate beds are thicker, nearly unconsolidated, and much less internally deformed than the strata of the Palm Spring Formation. The major anticline

371 displays an open, symmetric, partly box-shaped, NW–SE-trending, upright geometry with 2–
372 3° plunge of the fold axis to the northwest. Outcrops on the SW-dipping limb of the anticline
373 (Fig. 3c) are cut by a SW-dipping reverse fault system that is sub-parallel to the Indio Hills
374 fault (Supplement S5a). These reverse faults may be linked with the reverse fault in folded
375 strata of the Palm Spring Formation on the southeastern macro-fold back-limb described
376 above (Fig. 4). The upright geometry and sub-horizontal NW–SE-trending axes of related
377 small-scale folds in a mudstone layer (Fig. 4) resembles that of the SAFZ-parallel anticline.
378   A couple of major synclines showing axial traces parallel to the main San Andreas
379 fault are also well displayed on Google Earth images (Fig. 5 and Supplement S6). These folds
380 affect WSW-dipping strata of the Palm Spring Formation on the broadened western part of
381 the northwest and central macro-folds. Fold geometries are tight and asymmetric, with
382 wavelengths less than 200 meters, and presumably steep NW-plunging axes. The local
383 appearance and sheared geometry of these folds contrast both with the broad SAFZ-oblique
384 folds near the main San Andreas fault, and with that of the upright, SAFZ-parallel anticline
385 near the Indio Hills fault.
386
387 ***Major and minor faults***
388   Fold-related brittle faults exist both in granitic basement and in sedimentary rocks of
389 the Mecca and Palm Spring formations in the study area. Such faults display narrow damage
390 zones less than one meter wide and are geometrically either related to SAFZ-oblique or
391 SAFZ-parallel macro- and meso-scale folds, or are orthogonal to the SAFZ and related faults.
392 With exception of the main San Andreas and Indio Hills faults, brittle faults are generally
393 difficult to trace laterally but, where preserved, they display centimeter- to meter-scale strike-
394 slip and/or reverse dip-slip displacement. Macro-scale fault orientations and kinematics in
395 sedimentary rocks are more variable than in basement rocks, but strike commonly WNW–
396 ESE to N–S and show moderate–steep dips to the northeast (Fig. 2). Subsidiary meso-scale
397 faults include high-angle SW- and SE-dipping strike-slip faults, and low-angle SW-dipping
398 thrust faults. We describe the Indio Hills and main San Andreas faults, strike-slip faults, and
399 thrust faults in sedimentary strata, and fractures in basement rocks northeast of the Indio Hills
400 fault.
401 *Indio Hills and main San Andreas faults*
402   Along the Indio Hills fault, poor exposures make it difficult to measure fault strike and
403 dip directly , but Google Earth images suggest a rectilinear geometry in map view relative to
404 the uplifted sedimentary strata to the southwest (Fig. 2). The fault strikes mainly NW–SE and

405 is subparallel to the northeastern flank of the Indio Hills. Farther southeast, it probably merges

406 with the main San Andreas fault (Fig. 1; Tyler, 1974). In the southeastern part of the study

407 area (Fig. 2), the Indio Hills fault is most likely located between an outcrop of basement

408 granite and the first outcrops of overlying strata of the Palm Spring Formation. The granite

409 there is highly fractured and cut by vein and joint networks (see description below), as may be

410 expected in the damage zone of a major brittle fault.

411 Like the Indio Hills fault, fault-plane dip and strike of the main San Andreas fault

412 must be inferred indirectly. The main San Andreas fault in the study area strikes WNW–ESE

413 and is sub-vertical based on its consistent rectilinear surficial trace, and because it truncates

414 both back- and fore-limb strata on most of the SAFZ-oblique macro-folds (Fig. 2). Thus, the

415 main San Andreas fault does not seem to have had major impact on the initial geometry and

416 development of the macro-folds in the Indio Hills. However, notable exceptions include

417 displacement by the main San Andreas fault of the two shear folds on the southern flank of

418 the macro-folds (Fig. 5), and a consistent anticlockwise bend of most axial traces of the

419 macro-folds (Fig. 2).

420 *Strike-slip faults in folded sedimentary strata*

421 One major brittle fault set striking NW–SE and dipping steeply to the northeast has

422 developed on the central macro-fold (Figs. 3b and 6). The faults splay out from a bedding-

423 parallel core zone subparallel to steeply SW-dipping mudstone–siltstone layers on the

424 southern limb of the central macro-fold, and then proceed to truncate NW-dipping

425 sedimentary strata and offset the hinge of a macro-fold by c. 70 meters right-laterally before

426 dying out (Supplement S7a–b). The fault damage zone is traceable for more than one

427 kilometer along strike as a right-slip fault which displaces the hinge of a major, tight,

428 asymmetric, shear-like (similar style) fold (Fig. 6 and Supplement S8). The shear-folded

429 sedimentary strata bend clockwise toward the main fault, thus supporting dominant right-

430 lateral slip (Fig. 6). Minor faults branch out from the fault core zone and either die out in the

431 macro-fold hinge, and/or persist as bedding-parallel faults for some distance on the southern

432 limb of the macro-fold (Fig. 6).

433 At smaller scale, the folded and tilted strata of the Palm Spring Formation are

434 commonly truncated by sets of steep NW–SE-striking right-lateral and NNE–SSW-striking

435 left-lateral faults, displaying meter- to centimeter-scale offsets (Supplement S7b–d). These

436 minor faults generally dip steeply to the northeast to east-northeast, i.e., opposite to most

437 bedding surfaces, which dip southwest (Fig. 3b), and, in places, develop reddish fault gouge

438 along strike. Furthermore, these minor faults typically cut sandstone beds and flatten, and/or

439   die out within, mudstone beds, which restricts their lateral extent to a few decimeters–meters.

440   Kinematic indicators, such as offset of bedding surfaces and fold axial surfaces, yield mostly

441   right-slip displacements, in places with minor reverse components. In some localities, on fold

442   limbs within thick and competent sandstone beds, such minor right- and left-slip faults appear

443   to form conjugate sets (Supplement S7b and d) that may have developed simultaneously. In

444   addition, NNE–SSW-striking, ESE-dipping faults and/or semi-brittle kink bands sub-

445   orthogonal to the SAFZ are well displayed in the southeastern macro-fold (Fig. 3c and

446   Supplement S7e) and cut bedding surfaces at high angles with left-slip displacement,

447   therefore potentially representing cross faults between segments/splays of the SAFZ system.

448   *Reverse and thrust faults in folded sedimentary strata*

449   Reverse and thrust faults are common and traceable on the back-limb of the central

450   and southeastern macro-folds near the SAFZ-parallel anticline and the Indio Hills fault, but

451   not recorded in areas close to the main San Andreas fault. Reverse faults strike mainly NW–

452   SE and dip gently to the southwest, although subsidiary gently NE-dipping faults exist. An

453   example is the low-angle reverse fault that propagates out-of-the syncline on the southeastern

454   macro-fold (Fig. 4) and yields a NE-directed sense-of-shear. This thrust fault may continue

455   westward into the central macro-fold (Fig. 3b), where reverse offset of SW-dipping strata of

456   the Palm Spring Formation constrains vertical displacement from about 10–15 meters

457   (Supplement S5a), though offset is only of a few centimeters in the southeast (Fig. 4). This

458   fault system has a listric geometry, and internal splay faults die out in thick silt- to mud-stone

459   layers. The low-angle faults seem to develop almost consistently near major fold hinge zones

460   and propagate northeastward as out-of-the syncline thrusts (Fig. 4 and Supplement S5a).

461   In sandstone beds on the north-dipping limb of the major syncline, minor-scale thrust

462   faults, offset asymmetric fold hinges (Supplement S7c) and yield down-to-the-north (normal)

463   sense of shear if the strata are rotated to a horizontal position (Supplement S9). An opposite

464   effect is apparent for a conjugate set of minor normal faults in a small-scale graben structure

465   on the steep, north-dipping layer, which defines a set of reverse faults when rotating the

466   sedimentary strata to horizontal (Supplements S7d and S9).

467   *Fractures and faults in basement rocks north of the Indio Hills fault*

468   Basement-rock exposures in the Indio Hills are limited to a single, approximately 50-

469   m long chain of outcrops located in the southeasternmost part of the study area (Fig. 2). These

470   outcrops of massive granite are heavily fractured with mostly steep to sub-vertical sets that

471   strike dominantly NE–SW to ENE–WSW and subsidiary NW–SE to NNW–SSE (see

472   stereoplot in Fig. 2). Kinematic indicators are generally lacking, but in highly fractured areas,

473 centimeter-thick lenses of unconsolidated reddish gouge are present, comparable to fault

474 rocks observed in Palm Spring Formation sedimentary rocks and corresponding to similar

475 small-scale strike-slip and reverse faults in the basement granite. The fault sets in granitic

476 basement rocks trend parallel to fault sets in sedimentary strata southeast of the Indio Hills

477 fault (see stereoplots in Figure 2) and are therefore suggested to have formed due to similarly

478 oriented stress.

479

480 **Discussion**

481 *Structural evolution of SAFZ-oblique folds*

482   We mapped and analyzed three macro-scale fold systems between the Indio Hills and

483 main San Andreas faults. In map view (Fig. 2), the folds are right-stepping, and each fold set

484 is increasingly asymmetric (Z-shaped) and sigmoidal towards the Indio Hills fault in the

485 northeast. Based on these properties, we interpret the fold sets as modified SAFZ-oblique *en*

486 *echelon* macro-folds. Various investigators (Babcock, 1974; Miller, 1998; Titus et al., 2007;

487 Janecke et al., 2018; Bergh et al., 2019) describe similar fold geometries in sedimentary strata

488 from many other segments of the SAFZ and are interpreted as structures formed by right-

489 lateral displacement between two major fault strands. However, the present fold-orientation

490 data in the Indio Hills (Fig. 2) do not correspond with a uniform simple shear model in

491 between two active strike slip faults because the long axis of the strain ellipse is not

492 consistently about 45° to the shear zone as expected (Sanderson and Marchini, 1984;

493 Sylvester, 1988). Instead, fold geometries vary both across and along strike, e.g., axial surface

494 traces of dying-out macro-fold hinges are at high obliquity angles (> 50–65°) in the

495 southwest, whereas they are at much lower angles (< 20–30°) and merge with sigmoidal-

496 shaped patterns against the Indio Hills fault (Fig. 2). Thus, we propose that the SAFZ-oblique

497 macro-folds in Indio Hills rather evolved from a single boundary fault (Indio Hills fault)

498 being progressively more active through time. For example, a model in which the folds

499 initially splayed out from an early active Indio Hills fault through right-lateral distributed

500 displacement (compare with Titus et al., 2007) is consistent with fold hinges extending

501 outward south of the Indio Hills fault and dying out (broadening) away from the fault in a

502 several kilometer-wide damage zone (Fig. 2). Fold propagation outward from the Indio Hills

503 fault is supported by the increased structural complexity of the fold geometries towards the

504 Indio Hills fault. Furthermore, the initial upright, *en echelon* folding clearly occurred after

505 deposition of the entire Palm Spring Formation because of the involvement in folding of the

506 Bishop Ash and of adjacent strata possibly of the Ocotillo Formation (i.e., maximum age of

507   0.76 Ma – earliest late Pleistocene; Fig. 2 and Table 1). Should the whole Ocotillo Formation

508   be folded in the Indio Hills, the maximum age constraints could be narrowed to < 0.6–0.5 Ma

509   based on magnetostratigraphic ages for the upper part of the Ocotillo Formation (Kirby et al.,

510   2007). By contrast, the main San Andreas fault truncates both limbs of the open-style, *en*

511   *echelon* folds (Fig. 2), which therefore indicates younger deformation along this fault.

512   The moderate–steep westward plunge of all three macro-folds (≥ 30°), however,

513   shows that the presumed initial horizontal fold hinges rotated into a steeper plunge. Such

514   steepening may be due to, e.g., progressive shortening above a deep-seated fault, a hidden

515   splay of the Indio Hills fault, or to an evolving stage of distributed shortening (folding)

516   adjacent to the master strike-slip faults (e.g., Bergh et al., 2019), with gradually changing

517   stress–strain orientation through time, and/or due to structural tilting in the hanging wall of

518   the Indio Hills fault. This kind of fold reworking favors a situation where the northwestern

519   and central macro-folds were pushed up and sideways (right-laterally), following the

520   topography and geometry of an evolving transpressional uplift wedge (i.e., a contractional

521   uplift formed synchronously with successively with simple shear transpression to balance

522   internal forces in a crustal-scale critical taper; Dahlen, 1990). The corresponding eastward-

523   tightening, enhanced shear folding, and recurrent SW-directed overturned geometries of the

524   central macro-fold on the back-limb of the southeastern macro-fold near the Indio Hills fault

525   (Fig. 3b) support this idea.

526   We propose a progressive model that changes from distributed (*en echelon* folding) to

527   partly partitioned, i.e., pure shear (shortening) plus simple shear (strike-slip) deformation

528   (Fig. 7), as inferred for other parts of the SAFZ, e.g., in the Mecca Hills (Bergh et al., 2019).

529   In this model, the tight to isoclinal fold geometries to the northeast (Fig. 3b) may account for

530   progressively more intense shortening near the Indio Hills fault, whereas coeval strike-slip

531   faulting affected the already folded and steeply dipping strata of the lower Palm Spring

532   Formation (Fig. 6). This model would favor shortening to have evolved synchronously with

533   renewed strike-slip shearing adjacent to the Indio Hills fault, and/or on a blind fault below the

534   contact between the Mecca Formation and overlying Palm Spring Formation, because the

535   Mecca Formation is much less deformed (Fig. 3c). Alternatively, the more mildly deformed

536   character of the Mecca Formation conglomerate may arise from its homogeneity, which

537   contrasts with alternating successions of mudstone–siltstone and sandstone of the Palm Spring

538   Formation prone to accommodating large amounts of deformation and to strain partitioning.

539   Regardless, such reshaping of *en echelon* folds is supported by analog modelling (McClay et

540   al., 2004; Leever et al., 2011a, 2011b) suggesting that partly partitioned strain may lead to a

541   narrowing of fold systems near a major strike-slip fault (i.e., Indio Hills fault), whereas

542   widening away from the fault indicates still ongoing distributed deformation. Partly

543   partitioned deformation is supported by the tight to isoclinal and consistent Z-like geometry of

544   smaller-scale folds present on the back-limb of the central and southeastern macro-folds (Fig.

545   3b–c), indicating that they are all parasitic folds and related to the same partly partitioned

546   shear-folding event. Where S- and Z-like fold geometries are present, these minor folds may

547   have formed by buckling in an early stage of *en echelon* folding. An alternative interpretation

548   is that the tight, reshaped parasitic folds are temporally linked to the SAFZ-parallel macro-

549   fold south of the Indio Hills fault (Fig. 3c; see next section).

550

551   ***Structural evolution of SAFZ-parallel folds***

552   The SAFZ-parallel anticline differs significantly in geometry from the *en echelon*

553   macro-folds and associated parasitic folds by having an upright and symmetric geometry <

554   20° oblique to the Indio Hills fault. Thus, it resembles that of a fault-propagation fold in a

555   more advanced partitioned transpressional segment of the SAFZ (e.g., Titus et al., 2007;

556   Bergh et al., 2019). We suggest that this fold formed by dominant NE–SW-oriented

557   horizontal shortening, i.e., at high obliquity to the main Indio Hills fault (near-orthogonal pure

558   shear), and/or as a fault-related fold above a buried, major reverse (SW-dipping) oblique-slip

559   splay of the Indio Hills fault at depth (e.g., Suppe and Medwedeff, 1990). The timing might

560   be after the tight reworking of *en echelon* folds in the late Pleistocene. The idea of a late-

561   stage, highly oblique pure-shear overprint onto the macro-folds is supported by small-scale

562   upright folds located within the tight *en echelon* syncline on the back-limb of the modified

563   central macro-fold system (Fig. 4). The NW–SE trend, upright style, and negligible plunge of

564   the fold axes indicate that these folds may be superimposed on the steeper plunging and

565   reshaped *en echelon* folds, and/or that they formed in progression to an increased component

566   of NE–SW shortening on the Indio Hills fault. Nonetheless, these folds may have formed

567   simultaneously with the *en echelon* macro-folds in the (earliest?) late Pleistocene (Table 1)

568   due to uncertain (not fully understood) crosscutting relationships.

569   Progressive NE–SW-oriented contraction may have triggered formation of the upright

570   SAFZ-parallel anticline adjacent to the Indio Hills fault (Fig. 2 and 3c). The fault then acted

571   as a SW-dipping thrust fault with top-NE displacement. The oblique shortening then led to a

572   certain amount of uplift near the Indio Hills fault, and possibly also accomplished the

573   overturning of folds on the northeastern back-limb of the central and southeastern macro-fold.

574   A similar mode of advanced partitioned shortening was proposed for SAFZ-parallel fold

575 structures in central and southern California (Mount and Suppe, 1987; Titus et al., 2007;

576 Bergh et al., 2019). Our results are supported by stress orientation data acquired by Hardebeck

577 and Hauksson (1999) along a NE–SW-trending profile across the Indio Hills. They recorded

578 an abrupt change in the maximum horizontal stress direction from about 40° oblique to the

579 SAFZ around the main San Andreas fault, to about 70° oblique (i.e., sub-orthogonal) farther

580 northeast, near the Indio Hills fault, which supports the change in attitude and shape of macro-

581 fold geometries that we have outlined. Shortening and strike-slip partitioning, however, would

582 require synchronous right slip on another major fault strand, e.g., the main San Andreas fault,

583 a hypothesis that is supported by the recorded late-stage (i.e., late Pleistocene) shear folding

584 there (Fig. 5).

585

586 *Fold and fault interaction, evolution, and relative timing*

587 In this section we use the geometry and kinematics of folds and faults in the southern

588 Indio Hills to reconstruct the tectonic history of the area, not only of the inverted late

589 Cenozoic basin but also about strike-slip and dip-slip faults that bound the basin. Essential

590 tectonic events include (1) extensional normal faulting along the Indio Hills fault in the mid-

591 Miocene–Pliocene (ca. 15–3.0 Ma), (2) reactivation of the Indio Hills fault as a right-lateral to

592 oblique-reverse fault in the (earliest?) late Pleistocene to present-day (< 0.76 Ma), and (3)

593 right-lateral movement along the main San Andreas fault in the late Pleistocene to present-day

594 (< 0.76 Ma; Table 1).

595 Prior to inversion and uplift of the Indio Hills, the Indio Hills fault most likely acted as

596 a SW-dipping, extensional, basin-bounding normal fault. Indications of an early-stage episode

597 of extension are shown by micro-fault grabens in steeply dipping layers (Supplements S5d

598 and S6), by the deposition and preservation of sedimentary strata of the Palm Spring and

599 Mecca formations southwest of the Indio Hills, whereas they were eroded or never deposited

600 northeast of the fault, and by fining upwards of the stratigraphic units from conglomerates in

601 the Mecca Formation to coarse-grained sandstone in the lower parts of the Palm Spring

602 Formation. In addition, the flat geometry of micro thrust faults (e.g., Supplements S5b–c)

603 suggests that they were rotated during macro-folding. Restoration of all micro faults in their

604 initial position prior to macro-folding shows that some of these faults exhibit normal

605 kinematics with associated syn-tectonic growth strata (Supplements S5d and S9).

606 Alternatively, the Indio Hills fault dips northeast and uplifted the granitic basement rocks in

607 the hanging wall to the northeast, followed by erosion of the overlying Mecca, Palm Spring

608 and Ocotillo formations there (Fig. 1). We favor a basin geometry and formation similar to

that of the Mecca Hills, where down-SW slip along the Painted Canyon fault was inferred in the (Miocene?–) Pliocene (McNabb et al., 2017), and of the transtensional Ridge Basin though having opposite vergence (Crowell, 1982; Ehman et al., 2000) with a steep, SW-dipping normal fault that was progressively reactivated as an oblique-slip reverse/thrust fault during basin inversion. Formation of the Indio Hills fault as a normal fault probably occurred in mid-Miocene times during extension related to the opening of the Gulf of California (Stock and Hodges, 1989; Stock and Lee, 1994) as proposed for the Salton Trough (Dorsey et al., 2011 and references therein).

Right-lateral to right-lateral-reverse movement along the Indio Hills fault that led to the formation of the SAFZ-oblique *en echelon* macro-folds also supports a steeply dipping character for the precursory Indio Hills fault. The change to a right-lateral-reverse fault is further supported by the presence of both meso-scale strike-slip and thrust faults having similar NW–SE strikes (Fig. 4, and Supplements S4c and S5a). The increased reverse (and decreasing right-lateral) component of faulting may have triggered rotation of the *en echelon* macro-fold axes to a steeper plunge, reshaped the open asymmetric folds into tight overturned folds, and caused gentle buckling of strata in the nearby SAFZ-parallel anticline. Hence, the Indio Hills fault ultimately functioned as an oblique-slip thrust oblique to the transform plate boundary in the late Pleistocene, which is supported by oblique maximum horizontal stress near the Indio Hills fault (c. 70°; Hardebeck and Hauksson, 1999), while the main San Andreas fault simultaneously accommodated right slip during this period.

By contrast, the last episode of movement along the main San Andreas fault clearly postdates *en echelon* folding, from its truncating attitude (Fig. 2). In addition, the anticlockwise bending of the axial traces into an ENE–WSW trend towards the southwest suggests that a distributed component of off-fault deformation affected the area around the main San Andreas fault in its early kinematic stages in the late Pleistocene. The refolding of the southwest limb of the central macro-fold near the main San Andreas fault (Fig. 5) also favors a late-stage activation of this fault in the late Pleistocene (i.e., after the initial transpressional slip events along the Indio Hills fault in the – earliest? – late Pleistocene). Possibly as a consequence of a longer period of activity, and as suggested by relatively higher topographic relief and more intensely folded sedimentary strata in the vicinity of and along the Indio Hills fault than along the main San Andreas fault, the former probably accommodated significantly larger amounts of uplift than the latter. This implies a southwest-tilted geometry for the Indio Hills uplift.

Minor faults in the Indio Hills provide additional input to resolve the spatial, temporal and kinematic relations between macro-fold and fault interaction. We analyzed minor fault-related folds (Supplement S5c), which, in their current position on steep north-dipping beds, define down-to-the north displacement. However, when rotating the sedimentary strata to horizontal (Supplement S9), the fault-related folds define a low-angle fold-and-thrust system. These geometric relationships suggest that the minor folds and faults (other than right-slip faults) pre-date (or were coeval with) the SAFZ-oblique macro-folding event, and that they formed initially as internal fractures due to N–S-oriented shortening when the sedimentary strata were still horizontal. This implies that some partitioning (e.g., SAFZ-parallel small-scale thrust faults) occurred simultaneously with distributed deformation (e.g., SAFZ-oblique *en echelon* macro-folds).

Further, our field data suggest that minor right-slip faults evolved synchronously and parallel with the E–W-trending *en echelon* fold limbs, propagating through rheologically weaker mudstone beds that flowed plastically and acted as slip surfaces during distributed deformation. Later or simultaneously, these faults escaped from the mudstone beds and propagated as NW–SE-striking right-slip faults adjacent to tightened shear folds during partly partitioned deformation, and finally ended up with truncation of the SAFZ-oblique folds (Fig. 6 and Supplement S7a–c).

The presence of out-of-the syncline reverse/thrust faults relative to the reshaped and tightened SAFZ-oblique macro-folds (Fig. 4 and Supplement S5a and d), where SW-dipping thrust faults formed (sub-) parallel to the Indio Hills fault, and the related upright anticline (Fig. 3c) suggest successive distributed and partly partitioned strain in the study area. The proximity and superimposed nature of reverse/thrust faults relative to the reshaped *en echelon* folds suggest that they utilized modified fold hinges and steeply tilted limbs as preexisting zones of weakness. Despite the uncertainty around the crosscutting relationship between the SAFZ-parallel anticline and the SAFZ-oblique *en echelon* macro-folds, the low-angle thrust and intra-detachment folds in the southeastern macro-fold (Fig. 4) indicate that such thrust detachments may have already formed during (early?) distributed deformation, i.e., that distributed and partitioned deformation occurred simultaneously and/or progressively (see phases 1 and 2 in Table 1).

The conjugate WNW–ESE- to NNW–SSE-striking right-slip and NNE–SSW-striking left-slip faults and kink band features truncate strata on both macro-fold limbs (Fig. 3b–c) with an acute angle perpendicular to the macro-folded and tilted Palm Spring Formation strata

675   (e.g., Supplement S7e). Thus, they formed together with or after the *en echelon* macro-folding

676   (< 0.76 Ma).

677

678   ***Tectonic model***

679   In this section we use detailed structural analysis of folds and faults in the southeastern

680   Indio Hills to outline the structural history of the tectonic uplift itself, evaluate it in terms of

681   what is known about strain budgets within the southern San Andreas fault system, link it to

682   nearby structures (Eastern California shear zone and Landers–Mojave Line), and integrate the

683   local structural history into a structural synthesis for the southern San Andreas fault zone in

684   the past 4 Myr.

685   Our field and structural data support inversion and uplift of the Indio Hills involving

686   progressive or stepwise stages of folding and faulting, incorporating a switch from distributed

687   to partly partitioned transpression (Fig. 7). Prior to inversion in late Pleistocene time, the

688   Indio Hills fault may have been a steep, SW-dipping normal fault that downthrew (Miocene?–

689   ) Pliocene sedimentary strata against granitic basement rocks in its footwall to the northeast.

690   These basement rocks were partly eroded in the footwall of the fault. In the hanging wall of

691   the fault, strata of the Mecca Formation were deposited in the Pliocene, most likely at 3.7–3.0

692   Ma, and the lower and upper members of the Palm Spring Formation respectively at 3.0–2.3

693   Ma and 2.6–0.76 Ma, as suggested from paleomagnetic studies in the Mecca Hills (Chang et

694   al., 1987; Boley et al., 1994; McNabb et al., 2017).

695   Early inversion involved distributed transpressional strain triggered by right-lateral

696   slip along the Indio Hills fault (Fig. 7a). Three macro-scale, upright *en echelon* folds and

697   associated parasitic folds formed in loosely consolidated sedimentary rocks of the Mecca and

698   Palm Spring formations after the latter was deposited (< 0.76 Ma), i.e., probably in earliest

699   late Pleistocene time (Table 1). The fold set evolved oblique to the main strand of the SAFZ

700   and formed a right-stepping pattern of E–W-oriented axial surfaces that trend at a high angle

701   (45°) to the bounding Indio Hills fault due to uniform simple shear (e.g., Sanderson and

702   Marchini, 1984; Sylvester, 1988). This is notably observed in the less deformed southwestern

703   part of the study area (Fig. 2) near the main San Andreas fault, where the macro-folds still

704   display their initial non-plunging geometries. Bed-internal minor fold and fault systems in

705   weak mudstone beds (Fig. 4 and Supplement S5a) may have formed parallel to the E–W-

706   trending *en echelon* fold traces, either as thrust detachments due to oblique N–S shortening

707   when strata were horizontal, and/or as strike-slip faults on the fold limbs. In addition, minor

708   (bed-internal) SAFZ-parallel thrusts and folds formed prior to or together with the *en echelon*

709   macro-folds (Supplements S4b–c and S9a–b), thus suggesting minor strain partitioning.

710   Further deformation in the late Pleistocene led to gradual change from mostly

711   distributed with minor partitioned deformation to partly partitioned shortening and right-

712   lateral faulting and folding (Fig. 7b), probably since the Indio Hills fault started to

713   accommodate an increasing amount of reverse slip, thus acting as an oblique-slip right-lateral-

714   reverse fault, and where the main San Andreas fault did not yet play a major role. The main

715   result was tightening of the macro-folds toward the Indio Hills fault and clockwise rotation of

716   fold axes to a steeper westerly plunge due to increased shear folding, whereas *en echelon*

717   upright folding continued in the southwest (Fig. 7b). Increased shortening and shearing

718   reshaped the macro-folds and their back-limb folds to tight, isoclinal, and partly overturned

719   folds with consistent Z-style and sigmoidal axial-surface traces near the Indio Hills fault (Fig.

720   7b). The sigmoidal pattern of the WNW–ESE-trending *en echelon* macro-folds formed at a

721   much lower angle with the Indio Hills fault (< 20–$30°$) than farther southwest (60–70^0).

722   Furthermore, the incremental component of lateral strain is recorded as progressively

723   crosscutting NW–SE-striking, strike-slip shear faults terminating with local truncation of the

724   central macro-fold (see Fig. 7c and section below).Uplift of the Indio Hills in the late

725   Pleistocene (because the earliest late Pleistocene 0.765 Ma Bishop Ash is involved in folding;

726   Sarna-Wojcicki et al., 2000; Zeeden et al., 2014) was marked by a gradual switch to more

727   kinematically evolved transpressional strain partitioning, where the dominant shortening

728   component was accommodated by right-lateral-oblique, top-NE thrusting along the Indio

729   Hills fault and major strike-slip movement along the main San Andreas fault (Fig. 7c and

730   phase 3 in Table 1). NE-directed oblique thrusting on the Indio Hills fault and related minor,

731   reverse, out-of-the syncline faults led to uplift, which resulted in formation of a major

732   anticline parallel to the Indio Hills fault in sediments of the Mecca Formation (see anticline

733   closest to Indio Hills fault in Fig. 3c and 7c). With increasing partitioning, slip parallel to the

734   transform plate boundary was accommodated by right slip along the linear main San Andreas

735   fault, where sub-vertical folds formed locally, and presumed antithetic conjugate kink band

736   sets of right- and left-slip cross faults affected the entire uplifted area.

737   We favor a progressive evolution from distributed to partly partitioned deformation as

738   presented in Fig. 7a–c, although overlapping and synchronous formation of various structures

739   may have occurred (overlapping of phases 1 and 2 in Table 1), at least locally (except for the

740   late-stage main San Andreas fault and related shear folds; phase 3 in Table 1). The

741   overlapping and synchronous formation of structures is based on uncertainties in our field

data, e.g., variable cross-cutting relations of early, bedding-parallel strike-slip and thrust faults and *en echelon* macro-folds (Figs. 4 and 6, and Supplements S5c–d and S7), and from the spatial variations in the direction of maximum horizontal stress across the Indio Hills at present, from 40° oblique to the boundary faults near the main San Andreas fault to 70° oblique near the Indio Hills fault (Hardebeck and Hauksson, 1999).

Our observations of mostly lateral movement along the main San Andreas fault (i.e., southeastern continuation of the Mission Creek fault) and the proposed late Pleistocene to present-day age for deformation in the southeastern Indio Hills are consistent with work by Keller et al. (1982). A major difference between the northwestern and southeastern Indio Hills is the relatively tighter macro-folding over a narrower area and more intense character of deformation in between the two bounding faults in the southeastern Indio Hills (Figs. 2 and 3; Keller et al., 1982; Lancaster et al., 2012).

The right-lateral-reverse character of the Indio Hills fault and its role in our kinematic model for basin inversion in the southern Indio Hills are further supported by the relationship of the Indio Hills fault with the Eastern California shear zone, which merge together north of the study area where the Indio Hills fault bends into a NNW–SSE strike along the Landers–Mojave Line (Dokka and Travis, 1990a, 1990b; Nur et al., 1993a, 1993b; Thatcher et al., 2016). Recent activity along the Landers–Mojave Line recorded as six–seven earthquakes with M > 5 between 1947 and 1999 (Fig. 1; Nur et al., 1993a, 1993b; Du and Aydin, 1996; Spinler et al., 2010) indicates that a through-going NNW–SSE-striking fault crosscuts the Pinto Mountain fault (Nur et al., 1993a, 1993b; Rymer, 2000). Notably, the 1992 Joshua Tree earthquake occurred along the NNW–SSE-striking, west-dipping West Deception Canyon fault (Rymer, 2000 and references therein), which merges with the (probably southwest-dipping) Indio Hills fault in the south (see figure 1 in Rymer, 2000). Therefore, we propose that the Indio Hills fault, may be one of several faults to transfer displacement from unsuitably oriented, NW–SE-striking right-slip faults in the north, such as the Calico and Camp Rock faults, to the main SAFZ strand in the south (Fig. 1).

Farther southeast along strike, the Indio Hills and main San Andreas faults merge along a dextral freeway junction, i.e., a junction of three dextral fault branches (sensu Platt and Passchier, 2016 and Passchier and Platt, 2017), which may have enhanced wedge-shaped transpressional uplift of the Indio Hills after the late formation of the main San Andreas fault in the late Pleistocene (Fig. 8a–c and Table 1). However, anticlockwise rotation of the Indio Hills block and related structures in map view as predicted in a dextral freeway junction (Platt and Passchier, 2016; Passchier and Platt, 2017) was not recorded by our field data (except

776   along the main San Andreas fault due to localized right-slip along the fault; cf. sub-vertical

777   shear fold in Fig. 5). This may be due in part to the late formation of the main San Andreas

778   fault (< 0.76 Ma, i.e., late Pleistocene), i.e., clockwise rotation (in map view) of the fold and

779   fault structures due to right-lateral slip along the Indio Hills fault, and to the oblique-slip

780   character of the Indio Hills fault. Thus, the dextral freeway junction in the Indio Hills may be

781   more of a transitional nature. Instead of major anticlockwise rotation of the Indio Hills block

782   in map view, the accretion of material toward the fault junction due to right slip along the

783   main San Andreas fault is probably partly accommodated by the dominant vertical slip

784   component along the Indio Hills fault, leading to further uplift near the junction (i.e.,

785   clockwise rotation in cross section).

786

787   ***Regional comparison and implications***

788   The proposed progressive tectonic model for the Indio Hills uplift has wide

789   implications when compared and correlated with other fault strands of the SAFZ bounding

790   uplifted domains along strike in the Coachella and Imperial valleys (Fig. 8a–c), and in

791   explaining lateral variations in fault architectures, kinematic evolution and timing,

792   deformation mechanisms and areal segmentation (Sylvester and Smith 1987; McNabb et al.,

793   2017; Janecke et al., 2018; Bergh et al., 2019). Here we compare and contrast the structural

794   evolution of the southeastern Indio Hills with that of nearby tectonic uplifts (Mecca Hills and

795   Durmid Hills).

796   *Comparison with the Mecca Hills*

797   Previous studies of SAFZ-related uplifts between the Indio Hills and Durmid Hills in

798   Coachella Valley suggest that the Indio Hills and main San Andreas faults link up in the

799   southeasternmost Indio Hills and proceed as the main San Andreas fault in the Mecca Hills

800   (Fig. 8c) which then, together with the subsidiary Skeleton Canyon and Painted Canyon

801   faults, bounds a much wider flower-like uplift area than in the Indio Hills (Fig. 8c; Sylvester

802   and Smith, 1976, 1987; Sylvester, 1988; McNabb et al., 2017; Bergh et al., 2019). In contrast

803   to the Indio Hills fault, however, the main San Andreas fault in Mecca Hills has an

804   anastomosing geometry with thick (10–500 m), red-stained fault gouge. Regardless, we

805   consider these faults to be correlative and infer the lack of fault gouge along the Indio Hills

806   fault to be due to more localized strain on the Indio Hills fault than on the SAFZ in Mecca

807   Hills. This is supported by a more rectilinear geometry and lack of fold–fault linkage in Indio

808   Hills, which may have allowed initial lubrication of the fault surface in basement rocks with

809   high contrasting rheology (e.g., Di Toro et al., 2011; Fagereng and Beall, 2021), and which

810 hampered fluid circulation and extensive cataclasis. Another possible explanation may be the
811 presence of coarse-grained deposits of the Mecca Formation, which may have
812 partitioned/decoupled deformation along the Indio Hills fault from that in overlying Palm
813 Spring sedimentary strata.

814   Both the Indio Hills and Mecca Hills uplift areas are bounded to the northeast by a
815 presumed Miocene–Pliocene, SW-dipping normal fault (Fig. 8a), which later acted as major
816 SAFZ-parallel oblique-reverse faults, and which significantly contributed to the uplift of these
817 areas in (late) Pleistocene time (Sylvester and Smith, 1976, 1987; McNabb et al., 2017; Bergh
818 et al., 2019). In the Mecca Hills (Fig. 8c), the Painted Canyon fault is flanked in the hanging-
819 wall to the southwest by a basement-cored, macro-fold (Mecca anticline), which is similar to
820 the upright anticline that parallels the Indio Hills fault and adjacent minor thrust faults (Figure
821 2 & Figure *3*c and Supplement S5a). Similar folds appear adjacent to the Hidden Springs–
822 Grotto Hills fault (Sheridan et al., 1994; Nicholson et al., 2010), a NW–SE-striking, now
823 reverse splay fault of the main SAFZ between the Mecca Hills and Durmid Hills (Fig. 8c). It
824 is, however, unlikely that these marginal faults link up directly along strike. Rather, they
825 merge or splay with the SAFZ and SAFZ-oblique faults.

826   The inversion and main uplift history of the Mecca Hills segment of the SAFZ (Bergh
827 et al., 2019) initiated with right-lateral slip on a steep SAFZ, from where SAFZ-oblique *en*
828 *echelon* folds and dominantly right-slip faults splayed out in a one–two kilometers wide
829 damage zone on either side of the SAFZ (Fig. 8a). The subsidiary Skeleton Canyon fault
830 initiated as a steep right-lateral and SAFZ-parallel strike-slip fault along a small restraining
831 bend (Fig. 8b). Successive lateral shearing reshaped the *en echelon* folds into steeply plunging
832 folds with axial traces parallel to the SAFZ. The final kinematic stage generated SW-verging
833 fold and thrust structures parallel to the SAFZ (Fig. 8c), which truncated the *en echelon* folds
834 and the NE-dipping Skeleton Canyon fault. The resulting wedge-like flower structure thus
835 records a polyphase kinematic evolution from distributed, through locally partitioned, to fully
836 partitioned strain (Bergh et al., 2019).

837   Based on the geometric similarities, we consider that the *en echelon* macro-folds in
838 both Indio Hills and Mecca Hills formed coevally, but not on the same regional right-lateral
839 fault strand (Fig. 8a). In both areas, the *en echelon* folds and faults are strongly reworked and
840 tightened into sigmoidal shapes where they merge with the Indio Hills and Skeleton Canyon
841 faults respectively (Fig. 8b; Bergh et al., 2019), and SAFZ-parallel thrust faults formed early
842 (i.e., prior to macro-folding) both in the Indio Hills (Supplement S5c–d) and in the Mecca
843 Hills (Rymer, 1994), thus supporting continuous, partly partitioned strain field in both areas.

844 Strain partitioning caused major uplift of the Mecca Hills block along the Skeleton Canyon,

845 Painted Canyon, and Hidden Springs–Grotto Hills faults (Fig. 8c), all acting as SAFZ-parallel

846 oblique-slip thrust faults (Sheridan et al., 1994; Bergh et al., 2019). The partitioned right-slip

847 component was partly transferred to the main San Andreas fault in Indio Hills, and/or to an

848 unknown hidden fault southwest of the SAFZ (e.g., in Mecca Hills; Hernandez Flores, 2015;

849 Fuis et al., 2017), possibly the East Shoreline fault (Janecke et al., 2018).

850 Based on paleomagnetic and structural field studies, uplift of the SAFZ-related Mecca

851 basin started at ca. 2.6–0.76 Ma (i.e., earliest to mid Pleistocene) with partial and local erosion

852 of the Palm Spring Formation (see lower and upper unconformities in McNabb et al., 2017)

853 and culminated after 0.76 Ma (see unconformity between the uppermost Palm Spring

854 Formation and base of the Ocotillo Formation southwest of the Painted Canyon fault in

855 McNabb et al., 2017), i.e., after deposition of the whole Palm Spring Formation (McNabb et

856 al., 2017; Janecke et al., 2018). Uplift is still ongoing at present (Fattaruso et al., 2014;

857 Janecke et al., 2018). Fault activity and tectonic uplift of the Mecca Hills therefore most likely

858 initiated earlier (earliest Pleistocene) than in the Indio Hills (earliest late Pleistocene; Table

859 1), where the transition from the lower to the upper member of the Palm Spring Formation is

860 gradual and does not show any major unconformity.

861 *Comparison with Durmid Hills*

862 The Durmid ladder structure along the southern 30 kilometers of the SAFZ in Imperial

863 Valley defines a similar but oppositely merging, one–three kilometers wide wedge-shaped

864 uplift as in Indio Hills, bounded by the right-lateral and reverse East Shoreline fault to the

865 southwest and the main SAFZ to the northeast (Fig. 8c; Janecke et al., 2018). Internally, the

866 ladder structure comprises *en echelon* folds (Babcock, 1974; Bürgmann, 1991) that merge in a

867 sigmoidal pattern with the main SAF, and subsidiary sets of conjugate SAFZ-parallel right-

868 lateral and SAFZ-oblique E–W-striking, left-slip cross faults, which accommodated clockwise

869 rotation of internal blocks (Janecke et al., 2018). The *en echelon* folds formed at a comparable

870 time, i.e., < 0.76 Ma in the Indio Hills and at ca. 0.5 Ma in the Durmid Hills (Table 1). By

871 assuming a northwest continuation of the main SAFZ with the SAFZ in Mecca Hills, the East

872 Shoreline fault has no exposed correlative fault in the Mecca Hills and Indio Hills (Fig. 8c;

873 Damte, 1997; Bergh et al., 2019). Nevertheless, the East Shoreline fault may continue at depth

874 southwest of the main San Andreas fault (Janecke et al., 2018).

875 A significant difference between the Indio Hills–Mecca Hills and the Durmid Hills,

876 however, is the large number of cross faults in the Durmid ladder structure. Such faults are

877 interpreted as early-stage (ca. 1 Ma – early/mid Pleistocene), NE–SW-striking, left-lateral,

faults (Fig. 8a), which were rotated clockwise by progressive right-lateral motion into sigmoidal parallelism with the SAFZ and East Shoreline fault (Fig. 8b–c; Janecke et al. 2018). In contrast, cross faults in Indio Hills are much less common and, where present, probably formed late, but prior to the main San Andreas fault (i.e., in the earliest or middle part of the late Pleistocene). Thus, in the Indio Hills, there is no evidence of clockwise rotation of early-stage cross faults as in the Durmid Hills, but rather clockwise rotation of fold axial traces is common, which may be a first step in the formation of ladder-like fault blocks (e.g., Davis, 1999; Schultz and Balasko, 2003).

A major outcome of the comparison with Durmid Hills is that the wedge-shaped uplift block between the Indio Hills and main San Andreas faults may represent a failed uplift and/or the early stage of formation of a ladder structure. This idea is supported by presence of similar master faults and structures with comparable kinematics in both the Indio Hills and Durmid Hills, including oblique *en echelon* macro-folds, strike-slip faults acting as step-over faults, and reverse faults. Younger, non-rotated, conjugate cross faults exist in the Indio Hills but not in the Durmid Hills where such faults are more evolved features due to larger strain and more advanced stage of ladder structure formation. From these observations, one should expect to find ladder structures operating at different evolution stages among the many, yet unexplored uplifts in Coachella Valley.

Conclusions

1) The Indio Hills fault likely initiated as a SW-dipping, basement-seated normal fault during the opening of the Gulf of California in the mid Miocene, and was later inverted as a right-lateral reverse, oblique-slip fault in the (earliest?–) late Pleistocene due to transpression along the transform plate boundary, whereas the main San Andreas fault initiated probably as a dominantly right-slip fault during the later stages of uplift in the late Pleistocene.

2) The Indio Hills segment of the SAFZ in Coachella Valley, southern California evolved as a wedge-shaped uplift block between two major SAFZ-related fault strands, the Indio Hills and main San Andreas faults, which merge in a dextral freeway junction of a transitional nature to the southeast.

3) Transpressive deformation triggered uplift and inversion of the Indio Hills through a progressive change from distributed *en echelon* folding to partly partitioned right-slip thrusting. We favor a progressive rather than stepwise model in which the main uplift

was related to late shortening at the freeway junction where the Indio Hills and main San Andreas faults merge.

4) The Indio Hills fault is a splay fault of the SAFZ that merges to the north with the Landers–Mojave Line and contributes to transfer slip from unsuitably oriented faults of the Eastern California shear zone to the main San Andreas fault in the southeast.

5) A significant difference of the Indio Hills with the Durmid Hills is that left-lateral step-over and cross faults in the Durmid Hills rotated subparallel with the mSAF, whereas in Indio Hills, all cross faults are oblique with the SAFZ and, thus, may reflect an earlier stage of a still evolving ladder structure.

6) The initiation of right-lateral to right-lateral-reverse slip along major SAFZ-parallel faults and the main San Andreas fault in the Coachella Valley is younger towards the northwest (Pliocene in the Durmid Hills, early Pleistocene in the Mecca Hills and late Pleistocene in the Indio Hills). The onset of uplift, however, appears to be coeval in all tectonic uplifts (late to latest) Pleistocene.

Data availability

The structural dataset and field photographs used in the present study are available on DataverseNO (Open Access repository) at https://doi.org/10.18710/TM18UZ. Satellite and aerial images are from Google Earth (© Google Earth 2011).

Authors contribution

All authors contributed to collect structural measurements in the Indio Hills. JBPK wrote the first draft of the manuscript and designed half the figures and supplements (workload: 35%). Prof. SGB made major revision to the initial draft and designed half the figures and supplements (workload: 35%). Prof. AGS also revised the manuscript and provided major input about the local geology (workload: 30%).

Competing interests

The authors declare that they have no known competing interests.

Acknowledgments

The staff at the University of California–Santa Barbara and San Diego State University provided great hospitality during Steffen Bergh's sabbatical leaves in 2011–2012 and 2016–2017 while working with the San Andreas fault. We thank all the persons from

these institutions that were involved in this project. The authors thank Prof. Emeritus Arild
Andresen (University of Oslo) and Prof. Holger Stunitz (UiT) for helpful comments and Jack
Brown (San Diego State University) for fieldwork collaboration. Prof. Susanne Janecke (Utah
State University) and Dr. Miles Kenney (Kenney Geoscience) provided fruitful discussion.
We thank the reviewers (Dr. Jonathan Matti and an anonymous reviewer) for their extended
helpful comments on the manuscript.

Financial support

The present study is part of the CEED (Centre for Earth Evolution and Dynamics) and
ARCEx projects (Research Centre for Arctic Petroleum Exploration), which are funded by
grants from UiT The Arctic University of Norway in Tromsø and the Research Council of
Norway (grant numbers 223272 and 228107) together with eight academic and six industry
partners.

References

Allen, C. R.: San Andreas fault zone in San Gorgonio Pass, southern California, GSA Bull.,
68, 315–360, 1957.

Atwater, T. and Stock, J.: Pacific-North America Plate Tectonics of the Neogene
Southwestern United States: An Update, International Geology Review, 40:5, 375–
402, 1998.

Babcock, E. A.: Structural Geology and Geophysics of the Durmid Area, Imperial Valley,
California, Ph.D. Thesis, University of California, Riverside, 149 pp., 1969.

Babcock, E. A.: Geology of the northeast margin of the Salton Trough, Salton Sea, California,
GSA Bull., 85, 321–332, 1974.

Bergh S. G., Sylvester, A. G., Damte, A. and Indrevær, K.: Evolving transpressional strain
fields along the San Andreas fault in southern California: implications for fault
branching, fault dip segmentation and strain partitioning, Geophys. Res. Abs., 16,
EGU General Assembly, 24th April–2nd May, Vienna, Austria, 2014.

Bergh, S. G., Sylvester, A. G., Damte, A. and Indrevær, K.: Polyphase kinematic history of
transpression along the Mecca Hills segment of the San Andreas fault, southern
California, Geosphere, 15, 34 pp., 2019.

Bilham, R. and Williams, P.: Sawtooth segmentation and deformation processes on the
southern San Andreas fault, California, Geophys. Res. Lett., 12, 9, 557–560, 1985.

Blisniuk, K., Scharer, K., Sharp, W. D., Burgmann, R., Amos, C. and Rymer, M.: A revised position for the primary strand of the Pleistocene-Holocene San Andreas fault in southern California, Sci. Adv., 7, eaaz5691, 2021.

Boley, J.-L., Stimac, J. P., Weldon II, R. J. and Rymer, M. J.: Stratigraphy and paleomagnetism of the Mecca and Indio Hills, southern California, in: Geological Investigations of an Active Margin, edited by: McGill, S. F. and Ross, T. M., GSA, Cordilleran Section Guidebook, 27th Annual Meeting, San Bernardino County Museum Associations, USA, 336–344, 1994.

Bryant, W. A.: Fault number 118, Pinto Mountain fault zone (includes Morongo Valley fault), Quaternary fault and fold database of the United States, USGS website, 2000. https://earthquakes.usgs.gov/hazards/qfaults, accessed 05/03/2022 09:32 a.m.Bürgmann, R.: Transpression along the southern San Andreas fault, Durmid Hills, California, Tectonics, 10, 1152–1163, 1991.

Chang, S.-B. R., Allen, C. R. and Kirschvink, J. L.: Magnetic stratigraphy and a test for block rotation of sedimentary rocks within the San Andreas fault zone, Mecca Hills, southeastern California, Quat. Res., 27, 30–40, 1987.

Crowell, J. C.: The tectonics of the Ridge Basin, southern California, in: Geologic History of Ridge Basin, Southern California, SEPM, Pacific Section, 22, 25–42, 1982.

Dahlen, F. A.: Critical Taper Model of Fold-and-Thrust Belts and Accretionary Wedges, Annu. Rev. Earth Planet. Sci., 18, 55–99, 1990.

Dair, L. and Cooke, M. L.: San Andreas fault geometry through the San Gorgonio Pass, California, Geology, 37, 2, 119–122, 2009.

Damte, A.: Styles of deformation in zones of oblique convergence: Examples from the Mecca Hills, southern San Andreas fault, Unpublished Ph.D. thesis, University of California, Santa Barbara, 164 pp., 1997.

Davis, G. H.: Structural geology of the Colorado Plateau region of southern Utah, with emphasis on deformation bands, GSA Spec. Pap., 342, 157 pp., 1999.

Di Toro, G., Han, R., Hirose, T., De Paola, N., Nielsen, S., Mizoguchi, K., Ferri, F., Cocco, M. and Shimamoto, T.: Fault lubrication during earthquakes, Nature, 471, 494–498, 2011.

Dibblee, T. W. Jr.: Geology of the Imperial Valley, California, Californian Division of Mines Bulletin, 170, 21–28, 1954.

Dibblee, T. W. Jr.: Geology of the southeastern San Andreas fault zone in the Coachella Valley area, Southern California, in: Southern San Andreas fault, Whitewater to

Bombay Beach, Salton Trough, California, edited by: Baldwin, J., Lewis, L., Payne, M. and Rocquemore, G., South Coast Geological Society, Annual Field Trip Guide Book, 25, 35–56, 1997.

Dibblee, T. W. Jr. and Minch, J. A.: Geological map of the Thousand Palms & Lost Horse Mountain 15 minutes quadrangles, Riverside County, California, Dibblee Foundation, Map DF-372, 2008.

Dokka, R. K. and Travis, C. J.: Late Cenozoic strike-slip faulting in the Mojave Desert, California, Tectonics, 9, 311–340, 1990a.

Dokka, R. K. and Travis, C. J.: Role of the Eastern California Shear Zone in accommodating Pacific-North American plate motion, Geophys. Res. Lett., 17, 1323–1326, 1990b.

Dorsey, R. J., Housen, B. A., Janecke, S. U., Fanning, C. M. and Spears, A. L. F.: Stratigraphic record of basin development within the San Andreas fault system: Late Cenozoic Fish Creek–Vallecito basin, southern California, GSA Bull., 123, 5/6, 771–793, 2011.

Du, Y. and Aydin, A.: Is the San Andreas big bend responsible for the Landers earthquake and the eastern California shear zone, Geology, 24, 3, 219–222, 1996.

Ehman, ,K. D., Sullivan, M. D. and May, S. R.: Ridge Basin Field Trip Guidebook, Tectonic Controls on Facies Distribution and Stacking Patterns, Ridge Basin, southern California, SEPM, Pacific Section, Los Angeles, California, USA, 87, 50 pp., 2000.

Fagereng, Å. and Beall, A.: Is complex fault zone behavior a reflection of rheological heterogeneity, Phil. Trans. R. Soc. A329: 20190421, 2021.

Fattaruso L.A., M.L. Cooke & R.J. Dorsey. 2014. Sensitivity of uplift patterns to dip of the San Andreas fault in the Coachella Valley, California. Geosphere, vol. 10, pp. 1.12.

Fuis, G. S., Scheirer, D. S., Langenheim, V. E. and Kohler, M. D.: A New Perspective on the Geometry of the San Andreas Fault in Southern California and Its Relationship to Lithospheric Structure, BSSA, 102, 236–251, 2012.

Fuis G. S., Bauer, K., Goldman, M. R., Ryberg, T., Langenheim, V. E., Scheirer, D. S., Rymer, M. J., Stock, J. M., Hole, J. A., Catchings, R. D., Graves, R. W. and Aagaard, B.: Subsurface Geometry of the San Andreas Fault in Southern California: Results from the Salton Seismic Imaging Project (SSIP) and Strong Ground Motion Expectations, BSSA, 107, 4, 1642–1662, 2017.

Gold, P. O., Behr, W. M., Rood, D., Sharp, W. D., Rockwell, T. K., Kendrick, K. and Salin, A.: Holocene geologic slip rate for the Banning strand of the southern San Andreas

Fault, southern California, J. Geophys. Res. Solid Earth, 120.
doi:10.1002/2015JB012004

Groshong, R. H.: Strain, fractures, and pressure solution in natural single-layer folds, GSA
Bull., 86, 1363–1376, 1975.

Guest, B., Niemi, N. and Wernicke, B.: Stateline fault system: A new component of the
Miocene-Quaternary Eastern California shear zone, GSA Bull., 119, 11/12, 1337–
1346, 2007.

Hardebeck J.L. & E. Hauksson. 1999. Role of fluids in faulting inferred from stress field
signatures. Science, 285, pp. 236-239.

Hauksson, E., Yang, W. and Schearer, P. M.: Waveform Relocated Earthquake Catalog for
Southern California (1981 to June 2011), BSSA, 102, 5, 2239–2244, 2012.

Hernandez Flores, A. P.: Paleosismologia del sistema de fallas imbricado en la Sierra
Cucapah, Baja California, Mexico, Master's Thesis, Centre for Scientific Research and
Higher Education, Ensenada, Mexico, 254 pp., 2015.

Herzig, C. T., Mehegan, J. M. and Stelting, C. E.: Lithostratigraphy of the State 2-14
Borehole: Salton Sea Scientific Drilling Project, J. Geophys. Res., 93, B11, 12969–
l2980, 1988.

Janecke, S. U., Markowski, D. K., Evans, J. P., Persaud, P. and Kenney, M.: Durmid ladder
structure and its implications for the nucleation sites of the next M >7.5 earthquake on
the San Andreas fault or Brawley seismic zone in southern California, Lithosphere, 10,
5, 602–631, 2018.

Keller, E. A., Bonkowski, M. S., Korsch, R. J. and Schlemon, R. J.: Tectonic geomorphology
of the San Andreas fault zone in the southern Indio Hills, Coachella Valley, California,
GSA Bull., 93, 46–56, 1982.

Kirby, S. M., Janecke, S. U., Dorsey, R. J., Housen, B. A., Langenheim, V. E., McDougall, K.
A. and Steely, A. N.: Pleistocene Brawley and Ocotillo Formations: Evidence for
Initial Strike-Slip Deformation along the San Felipe and San Jacinto Fault Zones,
Southern California, J. of Geology, 115, 43–62, 2007.

Lancaster, J. T., Hayhurst, C. A. and Bedrossian, T. L.: Preliminary geologic map of
Quaternary surficial deposits in southern California: Palm Springs 30' x 60'
quadrangle, in: Geologic compilation of Quaternary surficial deposits in southern
California, edited by: Bedrossian, T. L., Roffers, P., Hayhurst, C. A., Lancaster, J. T.
and Short, W. R., California Geological Survey, Sacramento, December 2012.
https://www.conservation.ca.gov/cgs/fwgp/Pages/sr217.aspx#palmsprings.

1080   Leever, K., Gabrielsen, R. H., Sokoutis, D. and Willingshofer, E.: The effect of convergence

1081   angle on the kinematic evolution of strain partitioning in transpressional brittle

1082   wedges: Insight from analog modeling and high-resolution digital image analysis,

1083   Tectonics, 30, 2011a.

1084   Leever, K., Gabrielsen, R. H., Faleide, J. I. and Braathen, A.: A transpressional origin for the

1085   West Spitsbergen fold- and thrust belt: Insight from analog modeling, Tectonics, 30,

1086   1–24, 2011b.

1087   Lin, G.: Three-Dimensional Seismic Velocity Structure and Precise Earthquake Relocations

1088   in the Salton Trough, Southern California, BSSA, 103, 5, 2694–2708, 2013.

1089   Lin, G., Schearer, P. M. and Hauksson, E.: Applying a three-dimensional velocity model,

1090   waveform cross correlation, and cluster analysis to locate southern California

1091   seismicity from 1981 to 2005, J. Geophys. Res., 112, B12309, 2007.

1092   Lindsey, E. O. and Fialko, Y.: geodetic slip rates in the southern San Andreas Fault system:

1093   Effects of elastic heterogeneity and fault geometry, J. Geophys. Res., 118, 689–697,

1094   2013.

1095   Lutz, A. T., Dorsey, R. J., Housen, B. A. and Janecke, S. U.: Stratigraphic record of

1096   Pleistocene faulting and basin evolution in the Borrego Badlands, San Jacinto fault

1097   zone, Southern California, GSA Bull., 118, 11/12, 1377–1397, 2006.

1098   Markowski, D. K.: Confirmation of a New Geometric and Kinematic Model of the San

1099   Andreas Fault at Its Southern Tip, Durmid Hill, Southern California, Master's Thesis,

1100   Utak State University, Logan, USA, 151 pp., 2016.

1101   Matti, J. C., Morton, D. M. and Cox, B. F.: Distribution and geologic relations of fault

1102   systems in the vicinity of the Central Transverse Ranges, southern California, USGS

1103   Report, 85-365, 31 pp., 1985.

1104   Matti, J. C., Morton, D. M. and Cox, B. F.: The San Andreas fault system in the vicinity of

1105   the central Transverse Ranges province, southern California, U.S. Geological Survey

1106   Open-File, Report 92-354, 40 pp., 1992.

1107   Matti, J. C., and Morton, D. M.: Paleogeographic evolution of the San Andreas fault in

1108   southern California: a reconstruction based on a new cross-fault correlation, in: The

1109   San Andreas fault system: displacement, palinspastic reconstruction, and geologic

1110   evolution, edited by: Powell, R. E., Weldon, R. J. and Matti, J. C., GSA Mem., 178,

1111   107–159, 1993.

McClay, K. R., Whitehouse, P. S., Dooley, T. and Richards, M.: 3D evolution of fold and thrust belts formed by oblique convergence, Mar. Petrol. Geol. Bull., 21, 857–877, 2004.

McNabb, J. C.: Stratigraphic record of Pliocene-Pleistocene basin evolution and deformation along the San Andreas fault, Mecca Hills, California, Unpublished Master's Thesis, University of Oregon, 70 pp., 2013.

McNabb, J. C., Dorsey, R. J., Housen, B. A., Dimitroff, C. and Messé, G. T.: Stratigraphic record of Pliocene–Pleistocene basin evolution and deformation within the Southern San Andreas Fault Zone, Mecca Hills, California, Tectonophys., 719–720, 66–85, 2017.

Meere, P. A., Mulchrone, K. F. and Timmerman, M.: Shear fodling in low-grade metasedimentary rocks: Reverse shear along cleavage at a high angle to the maximum compressive stress, geology, 41, 8, 879–882, 2013.

Miller, D.D.: Distributed shear, rotation, and partitioned strain along the San Andreas fault, central California, Geology, 26, 867–870, 1998.

Morton, D., Matti, J. and Tinsley, J.: Banning fault, Cottonwood canyon, San Gorgonio pass, southern California, in: Cordilleran Section of the Geological Society of America, edited by: Hill, M., 191–192, Geol. Soc. of Am., Boulder, Colorado, USA, 1987.

Morton, D. and Matti, J. C.: Extension and contraction within an evolving divergent strike-slip fault complex: The San Andreas and San Jacinto fault zones at their convergence in southern California, in: The San Andreas fault system: displacement, palinspastic reconstruction, and geologic evolution, edited by: Powell, R. E., Weldon, R. J. and Matti, J. C., GSA Mem., 178, 217–230, 1993.

Mount, V. S. and Suppe, J.: State of stress near the San Andreas fault: implications for wrench tectonics, Geology, 15, 1143–1146, 1987.

Nicholson, C., Hauksson, E. and Plesch, A.: Revised 3D Fault Models for the Southern San Andreas Fault System Extending from San Gorgonio Pass to the Salton Sea, 106th Annual Meeting AAPG, 27th–29th May, 2010.

Nur, A., Hagai, R. and Beroza, G. C.: The Nature of the Landers-Mojave Earthquake Line, Science, 261, 201–203, 1993a.

Nur, A., Hagai, R. and Beroza, G. C.: Landers-Mojave earthquake Line: A New Fault System?, GSA Today, 3, 10, 255–258, 1993b.

Passchier, C. W. and Platt. J. P.: Shear zone junctions: Of zipper and freeways, J. Structural Geol., 95, 188–202, 2017.

1146 Platt, J. P. and Passchier, C. W.: Zipper junctions: A new approach to the intersections of
1147   conjugate strike-slip faults, Geology, 44, 10, 795–798, 2016.

1148 Rymer, M. J.: Quaternary Fault-Normal Thrusting in the Northwestern Mecca Hills, Southern
1149   California, GSA Cordilleran Section Guidebook, Trip 15, 268–272, 1994.

1150 Rymer, M. J.: Triggered Surface Slips in the Coachella Valley Area Associated with the 1992
1151   Joshua Tree and Landers, California, Earthquakes, BSSA, 90, 4, 832–848, 2000.

1152 Sanderson, D. J. and Marchini, W. R. D.: Transpression, J. Structural Geol., 6, 5, 449–458,
1153   1984.

1154 Sarna-Wojcicki, A. M., Pringle, M. S. and Wijbrans, J.: New ^{40}Ar/^{39}Ar age of the Bishop Tuff
1155   from multiple sites and sediment rate calibration for the Matuyama-Brunhes boundary,
1156   J. Geophys. Res., 105, B9, 21431–21443, 2000.

1157 Schultz, R. A. and Balasko, C. M.: Growth of deformation bands into echelon and ladder
1158   geometries, Geophys. Res. Lett., 30, 2033, 2003.

1159 Sheridan, J. M. and Weldon II, R. J.: Accomodation of compression in the Mecca Hills,
1160   California, GSA Cordilleran Section Guidebook, Trip 15, 273–279, 1994.

1161 Sheridan, J. M., Weldon II, R. J., Thornton, C. A. and Rymer, M. J.: Stratigraphy and
1162   Deformational History of the Mecca Hills, Southern California, GSA Cordilleran
1163   Section Guidebook, Trip 15, 262–268, 1994.

1164 Sieh, K., Jones, L., Hauksson, E., Hudnut, K., Eberhart-Phillips, D., Heaton, T., Hough, S.,
1165   Hutton, K., Kanamori, H., Lilje, A., Lindvall, S., McGill, S. F., Mori, J., Rubin, C.,
1166   Spotila, J. A., Stock, J., Kie Thio, H., Treiman, J., Wernicke, B. and Zachariasen, J.:
1167   Near-Field Investigations of the Landers Earthquake Sequence, April to July 1992,
1168   Science, 260, 171–176, 1993.

1169 Spinler, J. C., Bennett, R. A., Anderson, M. L., McGill, S. F., Hreinsdottir, S. and
1170   McCallister, A.: Present-day strain accumulation and slip rates associated with
1171   southern San Andreas and eastern California shear zone faults, J. Geophys. Res., 115,
1172   B11407, 2010.

1173 Spotila, J. A., Niemi, N., Brady, R., House, M., Buscher, J and Oskin, M.: Long-term
1174   continental deformation associated with transpressive plate motion: The San Andreas
1175   fault, Geology, 35, 11, 967–970, 2007.

1176 Stock, J. M. and Hodges, K. V.: Pre-Pliocene extension around the Guld of California and the
1177   transfer of Baja California to the Pacific plate, Tectonics, 8, 1, 99–115, 1989.

1178 Stock, J. M. and Lee, J.: Do microplates in subduction zones leave a geological record?,
1179   Tectonics, 13, 6, 1472–1487, 1994.

1180   Suppe, J. and Medwedeff, D. A.: Geometry and kinematics of fault-propagation folding,

1181   Eclogae geol. Helv., 83/3, 409–454, 1990.

1182   Sylvester, A. G.: Strike-slip faults, GSA Bull., 100, 1666–1703, 1988.

1183   Sylvester, A. G. and Smith, R. R.: Tectonic Transpression and Basement-Controlled

1184   Deformation in San Andreas Fault Zone, Salton Trough, California, Treatise of

1185   Petroleum Geology, 60, 12, 2081–2102, 1976.

1186   Sylvester, A. G. and Smith, R. R.: Structure section in Painted Canyon, Mecca Hills, southern

1187   California, GSA Centennial Field Guide, Cordilleran Section, 103–108, 1987.

1188   Sylvester, A. G., Bilham, R., Jackson, M. and Barrientos, S.: Aseismic Growth of Durmid

1189   Hill, Southeasternmost San Andreas Fault, California, J. Geophys. Res., 98, B8,

1190   14233–14243, 1993.

1191   Titus, S. J., Housen, B. and Tikoff, B.: A kinematic model for the Rinconada fault system in

1192   central California based on structural analysis of en echelon folds and

1193   paleomagnetism, J. Struct. Geol., 29, 961–982, 2007.

1194   Thatcher, W., Savage, J. C. and Simpson, R. W.: The Eastern California Shear Zone as the

1195   northward extension of the southern San Andreas Fault, J. Geophys. Res., Solid Earth,

1196   121, 2904–2914, 2016.

1197   Tyley, S. J.: Analog model study of the ground-water basin of the upper Coachella Valley,

1198   California, U.S. Geological Survey Water-Supply, 2027, 1974.

1199   Vollmer, F. W.: Orient 3: a new integrated software program for orientation data analysis,

1200   kinematic analysis, spherical projections, and Schmidt plots, GSA Abstracts with

1201   Programs, 47, 7, 49, 2015.

1202   Winker, C. D. and Kidwell, S. M.: Stratigraphy of a marine rift basin: Neogene of the western

1203   Salton Trough, California, in: Field Conference Guide, edited by: Abbott, P. L. and

1204   Cooper, J. D., AAPG National Convention, San Diego, California, USA, 295–336,

1205   1996.

1206   Zeeden, C., Rivera, T. A. and Storey, M.: An astronomical age for the Bishop Tuff and

1207   concordance with radioisotopic dates, Geophys. Res. Lett., 41, 3478–3484, 2014.

1208 **Figures**

1209

1210
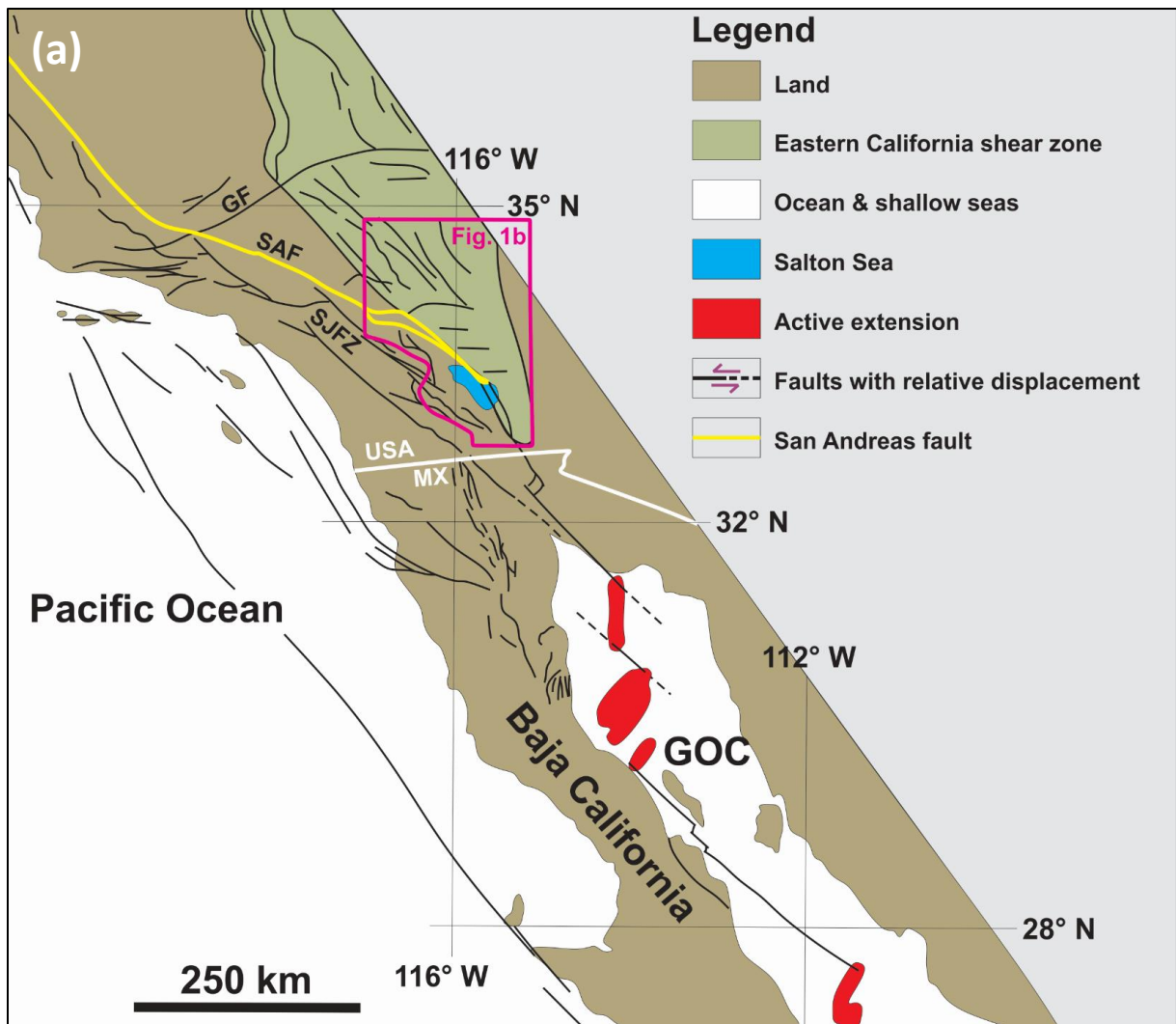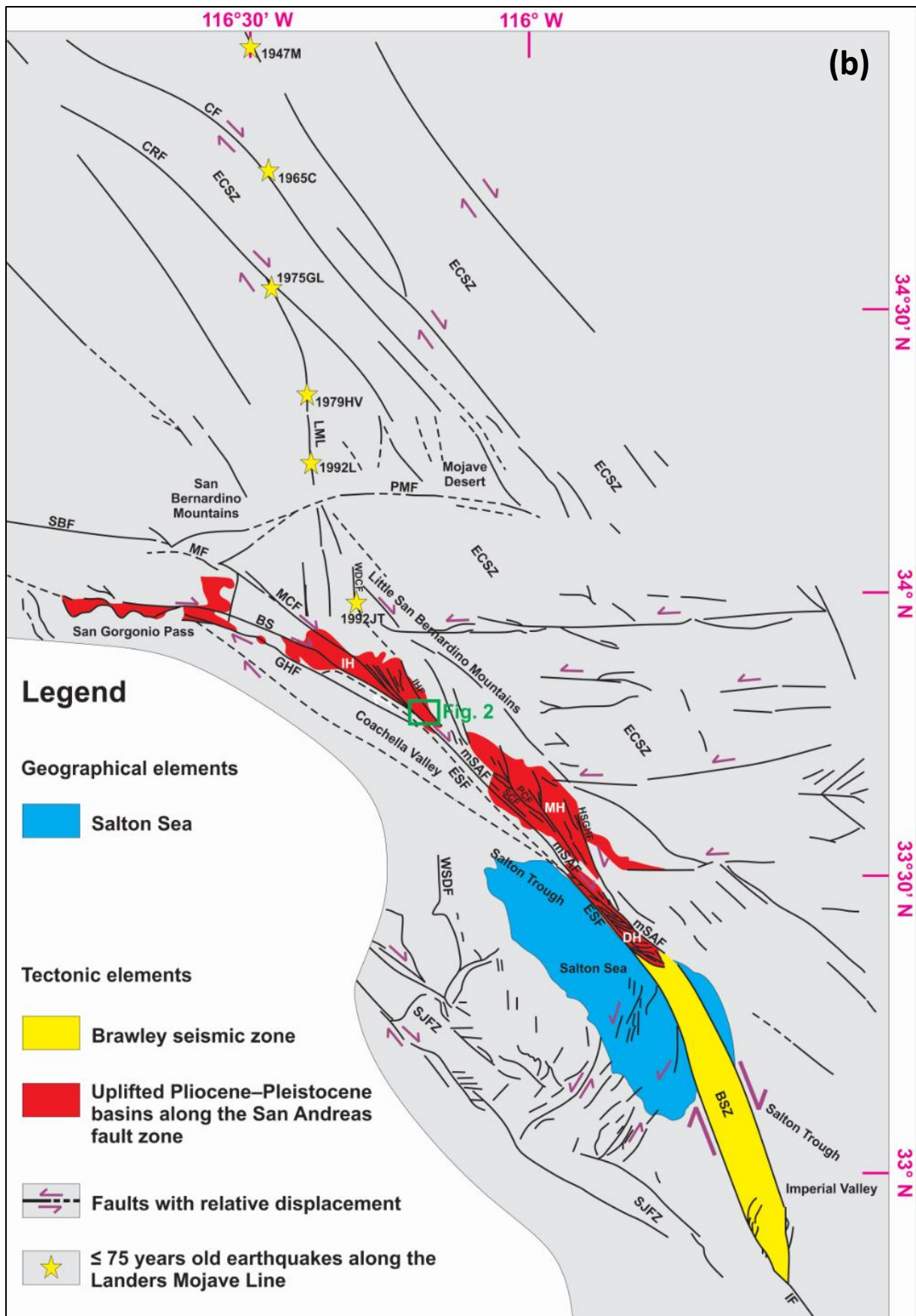
Figure 1: (a) Map of the main geological features of southern California, Baja California and the Gulf of California. The location of (b) is shown as a fuchsia polygon. Modified after Janecke et al. (2018). (b) Simplified geological map of the Coachella Valley and Salton Trough, southern California, showing the three main transpressional uplift areas along the SAFZ: the Indio Hills (IH), Mecca Hills (MH), and Durmid Hills (DH). Note the link of the SAFZ with the Brawley seismic zone to the south. The study area is shown in a green rectangle. Recent earthquakes (≤ 75 years) along the Landers–Mojave Line (LML) are shown as yellow stars with associated year of occurrence. Faults are drawn after Rymer (2000), Guest et al. (2007), Janecke et al. (2018), and Bergh et al. (2019). Earthquakes after Nur et al. (1993a, 1993b). Abbreviations: 1947M: 1947 Manix earthquake; 1965C: 1965 Calico earthquake; 1975GL: 1975 Galway Lake earthquake; 1979HV: 1979 Homestead Valley earthquake; 1992JT: 1992 Joshua Tree earthquake; 1992L: 1992 Landers earthquake; BS: Banning strand; BSZ: Brawley seismic zone; CF: Calico fault; CRF: Camp Rock fault; DH: Durmid Hills uplift; ECSZ: Eastern California shear zone; ESF: East Shoreline fault; GF: Garlock fault; GHF: Garnet Hill fault; GOC: Gulf of California; HSGHF: Hidden Springs–Grotto Hills fault; IF: Imperial fault; IH: Indio Hills uplift; IHF: Indio Hills fault; LML: Landers–Mojave Line; MCF: Mission Creek fault; MF: Mill Creek fault; MH: Mecca Hills uplift; mSAF: main San Andreas fault; PCF: Painted Canyon fault; PMF: Pinto Mountain fault; SBF: San Bernardino fault; SCF: Skeleton Canyon fault; SJFZ: San Jacinto fault zone; WDCF: West Deception Canyon fault; WSDF: West Salton detachment fault.
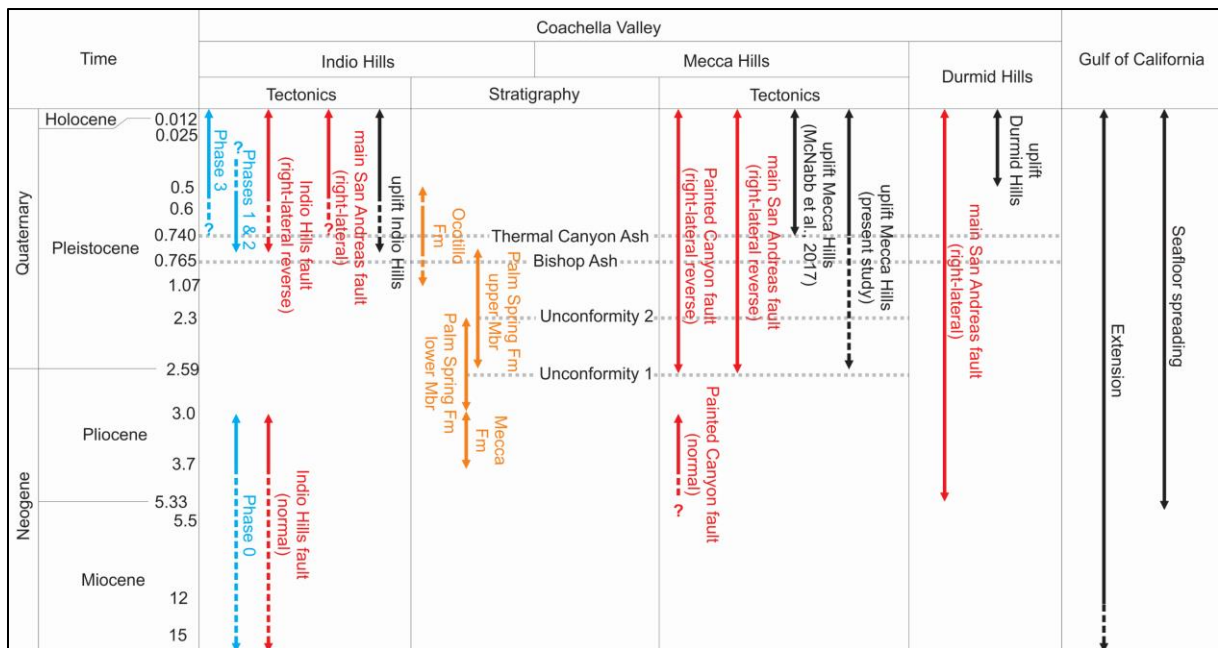
1232

1233 **Table 1: Summary of the timing of the main events in the Coachella Valley and Gulf of**

1234 **California. Note the presumed timing phases (1-3) of fold-faulting and uplift events in**

1235 **the Indio Hills (this work). The stratigraphy is common to the Mecca Hills and Indio**

1236 **Hills, although some features are only observed in one area (e.g., unconformities 1 and 2**

1237 **in the Mecca Hills but not in the Indio Hills).**
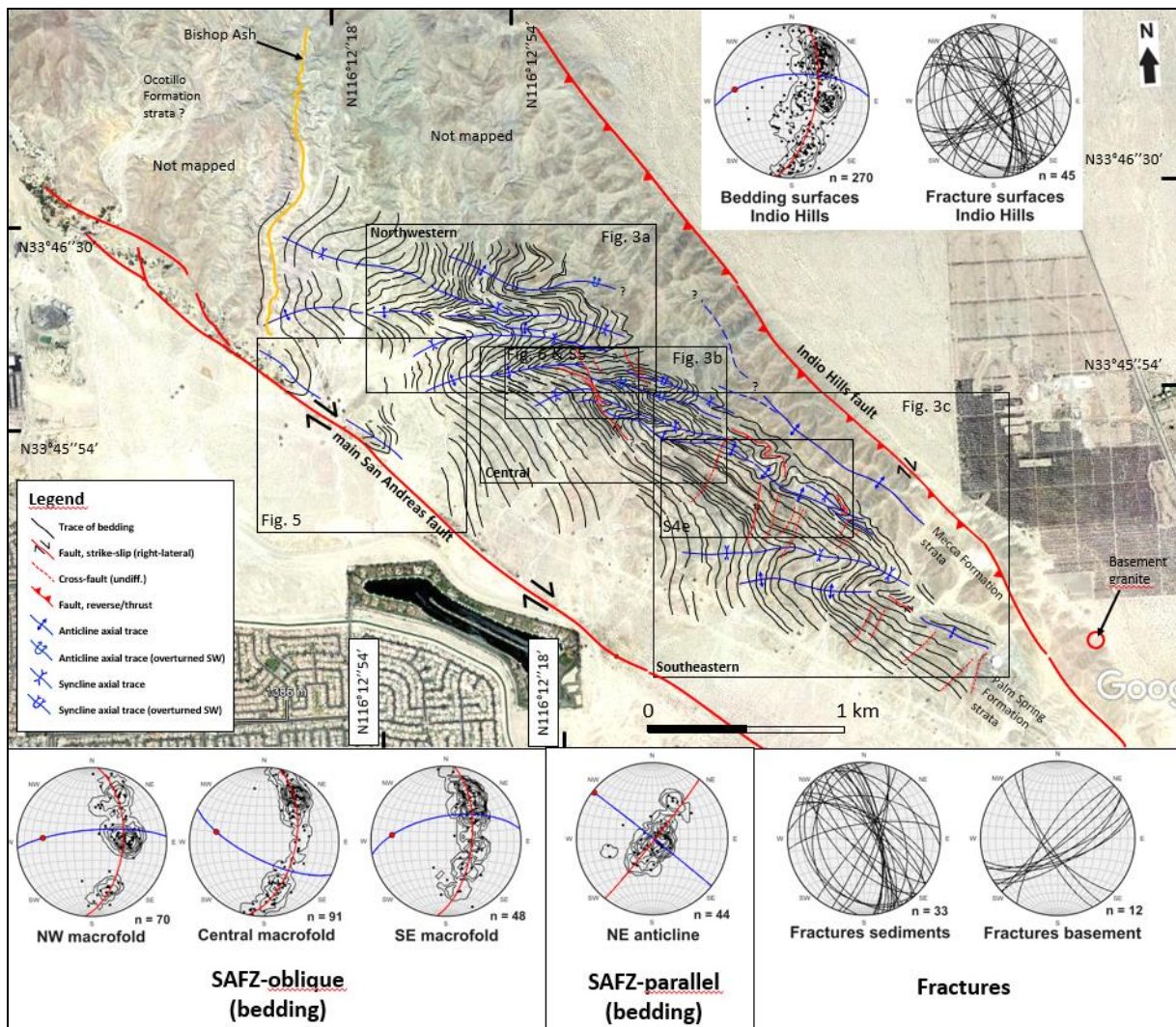
Figure 2: Interpreted Google Earth image in the southeastern part of the Indio Hills uplift area. Three main SAFZ-oblique macro-folds (northwestern, central, southeastern) are mapped in between the bounding Indio Hills and main San Andreas faults, whereas one SAFZ-parallel anticline is present close to the Indio Hills fault. More detailed figures are numbered and framed. Structural datasets are plotted in lower hemisphere Schmidt stereonets via the Orient software (Vollmer, 2015). Note that faults are also included as fractures in the stereonets. Bedding surfaces are shown as pole to plane with frequency contour lines, with average πS great circle (red great circles), fold axial surface (blue great circles) and fold axis (red dots). Brittle fractures in sedimentary strata and basement rocks are plotted as great circles. Source: Google Earth historical imagery 09-2011. Uninterpreted version of the image available as Supplement S1. © Google Earth 2011.
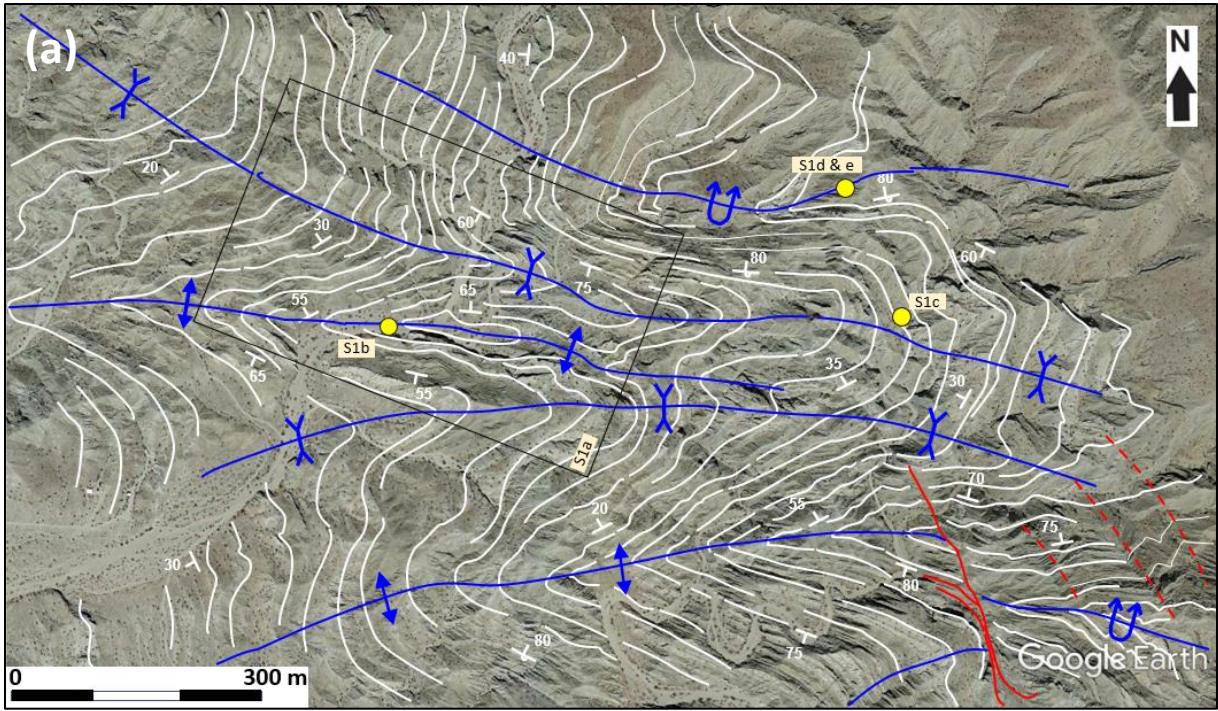
1251
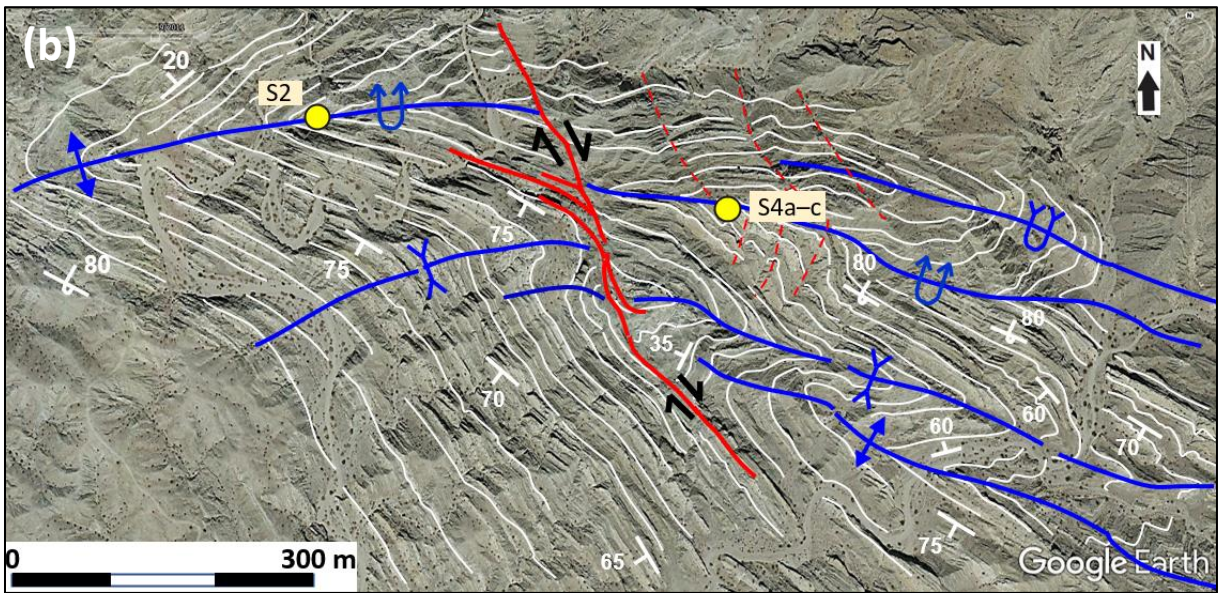
1252
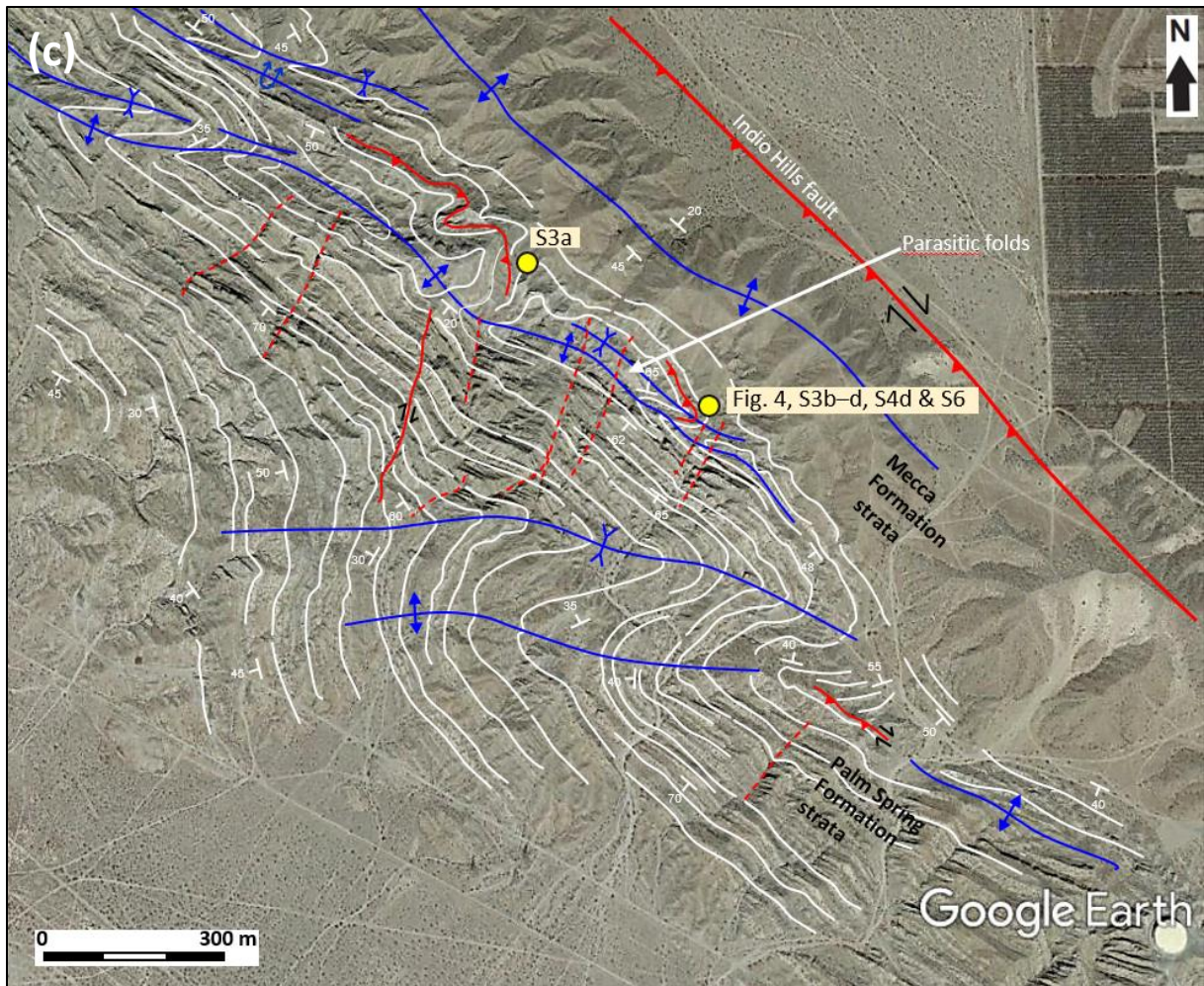
1253

**Figure 3: Detailed structural maps showing the architecture and outline of anticline-
syncline pairs, traces of bedding and strike and dip orientation, axial surface traces, and
fold-related faults in (a) the northwestern, (b) central, and (c) southeastern macro-folds.
Note tighter and consistently asymmetric (Z-shaped) geometries of the macro-folds to
the east, whereas folds to the west are more open and symmetric. Traces and orientation
of bedding show a back-limb composed of attenuated shear folds merging from the
central macro-fold in the north, whereas the fore-limb is much shorter and more
regularly folded. The yellow dots show the location of field photographs. See fig. 2 for
legend and location. Uninterpreted version of the images available as Supplement S2a–c.
© Google Earth 2011.**
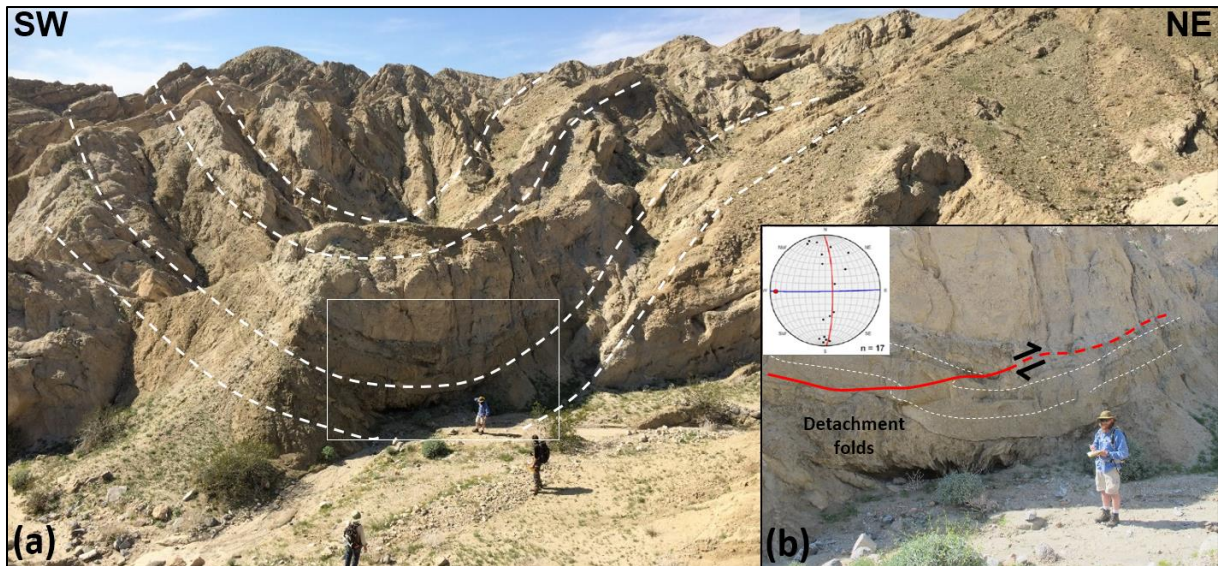
1264

1265 **Figure 4: Meso-scale folds and related faults on the back-limb of the southeastern**

1266 **macro-fold. See location in fig. 3c. (a) Syncline in upper Palm Spring Formation units**

1267 **adjacent to the SAFZ-parallel macro-fold near the Indio Hills fault. (b) Close-up view of**

1268 **the synclinal fold hinge in (a), where a meter thick sandstone bed is slightly offset by a**

1269 **minor, low-angle thrust fault (red line) with NE-directed sense-of-shear. The minor**

1270 **thrust faults die out in the overlying sandstone bed. The mudstone bed below acts as a**

1271 **décollement layer with internal, plastically folded lamination, including disharmonic,**

1272 **intra-detachment folds. Structural orientation data of minor, centimeter-scale fold limbs**

1273 **in the décollement zone are plotted in a lower hemisphere Schmidt stereonet, indicating**

1274 **E–W-trending fold axes and a sub-horizontal axial surface (average great circle in red**

1275 **and fold axis as a red dot).**
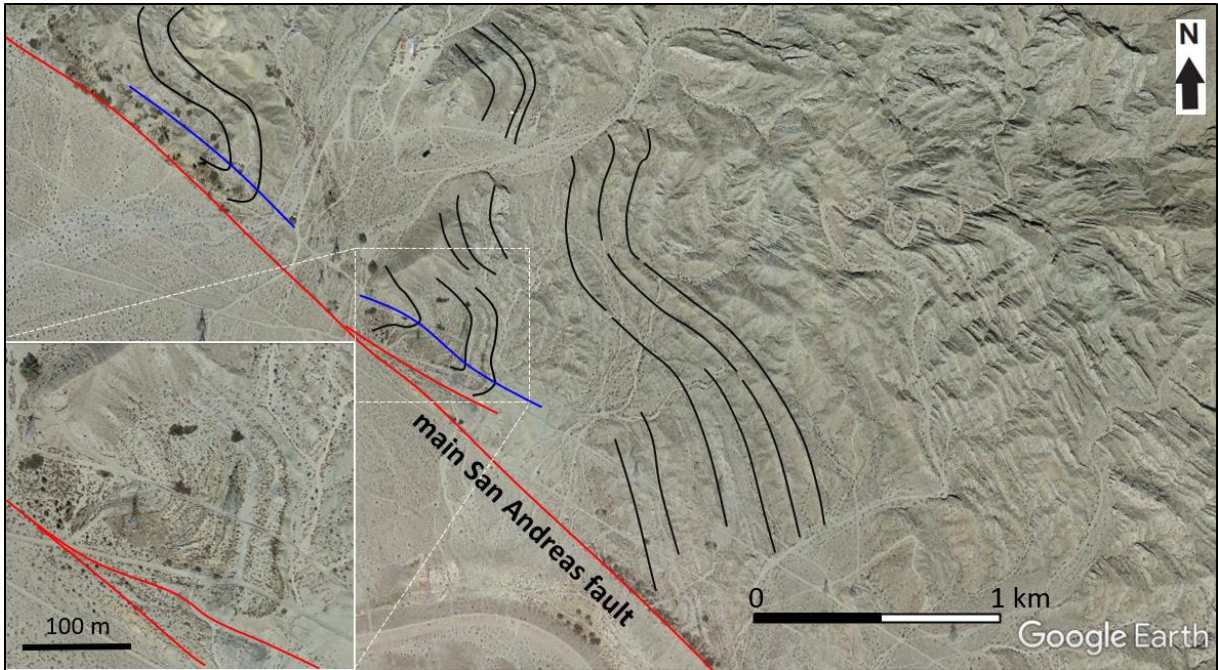
Figure 5: Interpreted SAFZ-parallel macro-folds (synclines) adjacent to the main San Andreas fault, which affect the southern limb of earlier (*en echelon*) macro-folded and tilted strata of the Palm Spring Formation. Note shear fold geometry in inset map with a thickened hinge zone and thinned limb to the south, steeply plunging axis, and axial trace parallel to the main San Andreas fault. See fig. 2 for location. Uninterpreted version of the image available as Supplement S4. © Google Earth 2011.
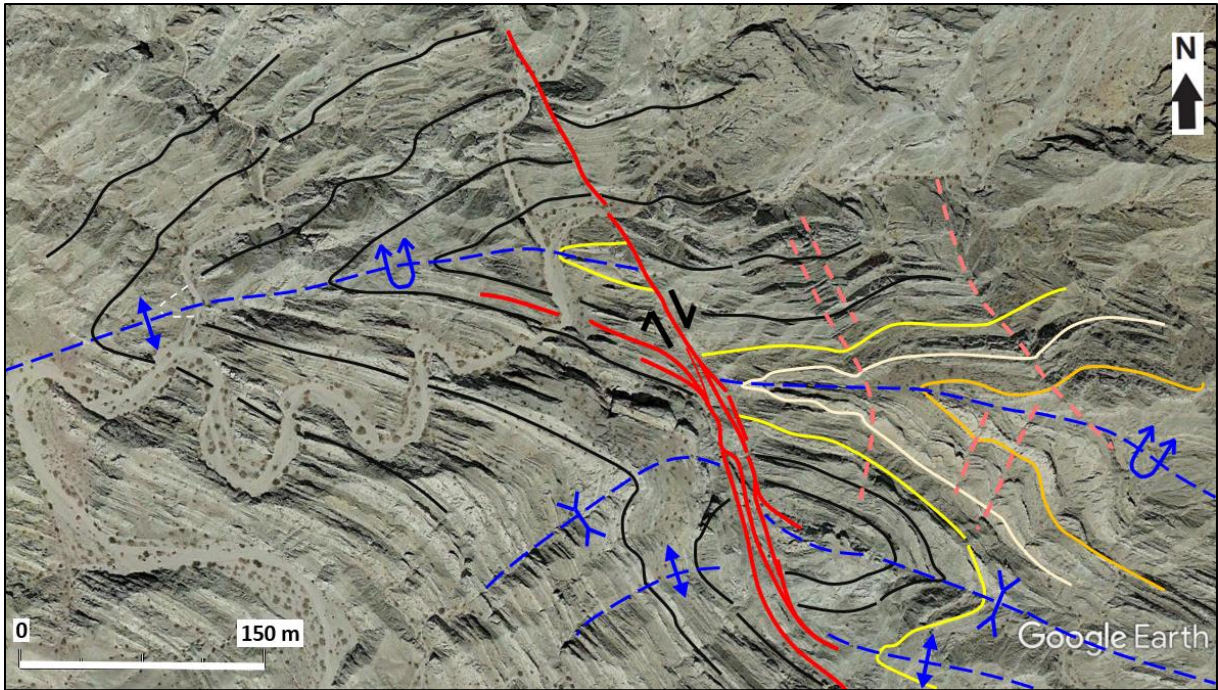
Figure 6: Interpreted satellite image of the central macro-fold showing right-lateral offset of the entire fold hinge/axial surface (upper left dashed blue line) by a NNW–SSE-trending, NE-dipping strike-slip fault (red lines). Note that the fault merges out from a layer in the southern limb of the macro-fold (black lines) and continues as a right-lateral fault. Offset geological markers include thick sandstone beds (yellow, white, light brown lines) and the fold axial surfaces of a second syncline fold farther south (lower right, dashed blue lines). Note that the syncline axial trace dies out to the southwest, and that kink bands acting as cross faults crop out in the eastern part of image (dashed pink lines). Uninterpreted version of the image available as Supplement S8. © Google Earth 2011.
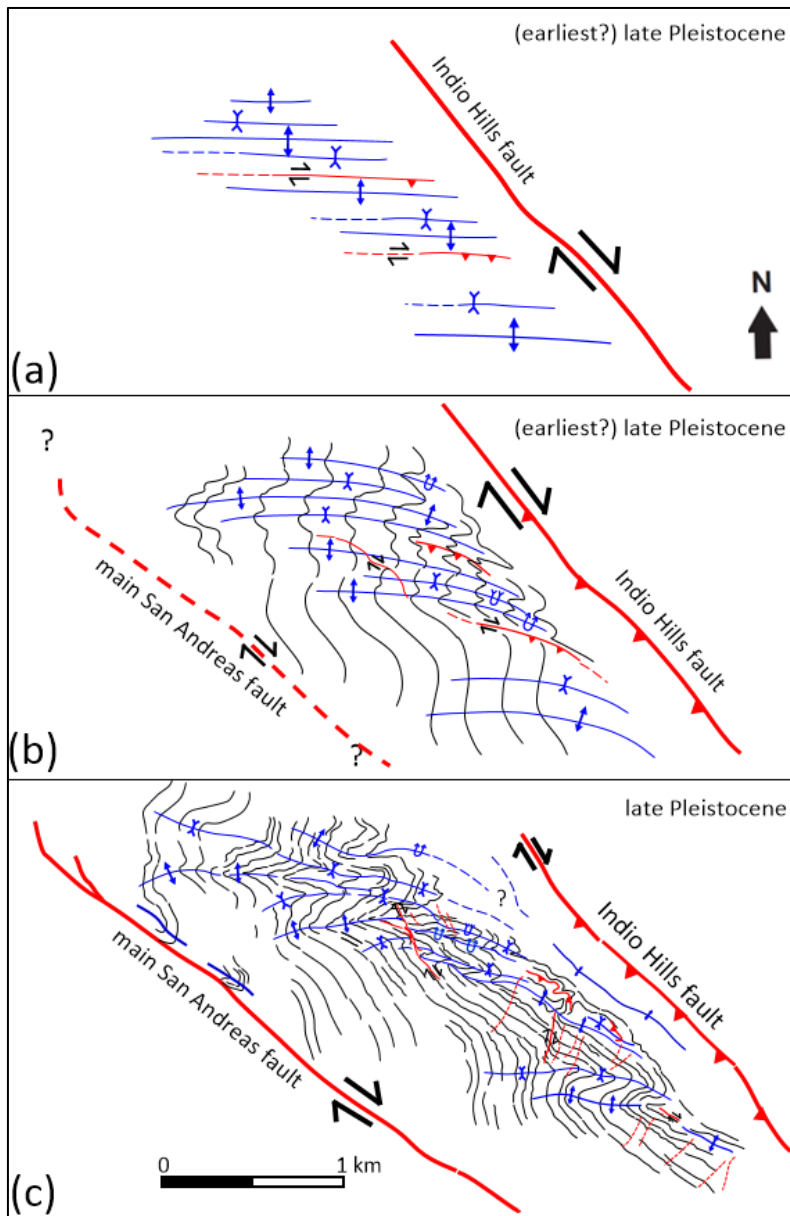
Figure 7: Model illustrating the progressive uplift/inversion history of the Indio Hills presuming a narrow time interval between formation of all structures in the area, except for the main San Andreas fault and associated folds. (a) Early distributed transpressional strain and formation of three major, *en echelon* **oriented macro-folds, several subsidiary parasitic anticline-syncline fold pairs, and bed-parallel strike-slip and reverse (décollement) faults initiating at a high angle (c. 45°) to the Indio Hills fault. (b) Incremental partly partitioned transpression when the Indio Hills fault started to accommodate oblique-reverse movement forcing previous horizontal** *en echelon* **macro-folds and parasitic folds to tighten, overturn, and rotate into steeper westward plunges. Note also sigmoidal rotation of axial traces on the back-limbs of the macro-folds to low angle (< 20–30°) with the Indio Hills fault. (c) Late-stage advanced strain partitioning**

1306   **with dominant shortening component on the oblique-reverse Indio Hills fault, and right-**

1307   **lateral slip on the main San Andreas fault. Notice the formation of the anticline parallel**

1308   **to the Indio Hills fault, subsidiary fold-internal strike-slip faults, and conjugate cross**

1309   **faults and kink bands that overprinted the macro-folds. Legend as in fig. 2.**
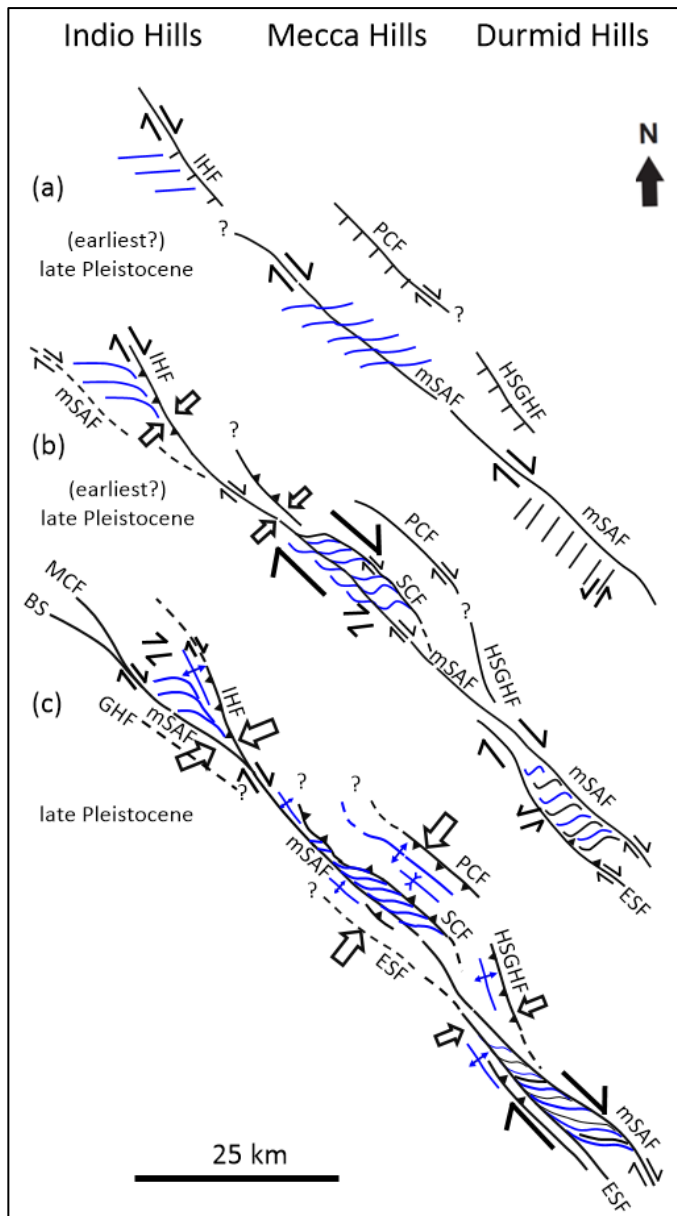
Figure 8: Kinematic evolution, timing, and along-strike correlation of the Indio Hills, Mecca Hills, and Durmid Hills uplift domains and bounding master faults in the Coachella valley, southern California. We present a progressive kinematic evolution from (a) distributed, through (b) partly partitioned, to (c) advanced partitioned strain events. See text for further explanation. Black lines are faults (full or stippled). Blue lines are fold axial traces. Wide arrows indicate main shortening direction, half-arrows lateral (strike-slip) shearing. Abbreviations: BS: Banning strand; ESF: East Shoreline fault; GHF: Garnet Hill fault; HSGHF: Hidden Springs–Grotto Hills fault; IHF: Indio Hills fault; mSAF: main San Andreas fault; MCF: Mission Creek fault; PCF: Painted Canyon fault; SCF: Skeleton Canyon fault.